

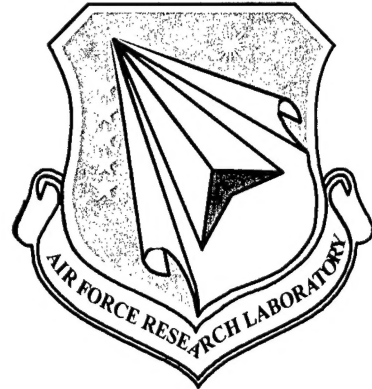
AFRL-MN-EG-TR-2001-7023

**Development of a Conservative Integration Scheme for the  
Equations of Hydrodynamics Using Unstructured Grids**

---

Michael L. Stokes

Mississippi State University  
Engineering Research Center  
Box 9627  
Mississippi State, MS 39762-9627



GRANT NO. FO8630-98-1-0004

April 2001

FINAL REPORT FOR PERIOD May 1998 - September 2000

**DISTRIBUTION A.** Approved for public release; distribution unlimited.

**AIR FORCE RESEARCH LABORATORY, MUNITIONS DIRECTORATE**

**Air Force Materiel Command    United States Air Force    Eglin Air Force Base**

**20010813 033**

# REPORT DOCUMENTATION PAGE

Form Approved  
OMB No. 0704-0188

Public reporting burden for this collection of information is estimated to average 1 hour per response, including the time for reviewing instructions, searching existing data sources, gathering and maintaining the data needed, and completing and reviewing the collection of information. Send comments regarding this burden estimate or any other aspect of this collection of information, including suggestions for reducing this burden, to Washington Headquarters Services, Directorate for Information Operations and Reports, 1215 Jefferson Davis Highway, Suite 1204, Arlington, VA 22202-4302, and to the Office of Management and Budget, Paperwork Reduction Project (0704-0188), Washington, DC 20503.

1. AGENCY USE ONLY (Leave blank)

2. REPORT DATE  
April 2001

3. REPORT TYPE AND DATES COVERED  
Final May 1998 – September 2000

4. TITLE AND SUBTITLE

Development of a Conservative Integration Scheme for the Equations of Hydrodynamics Using Unstructured Grids

5. FUNDING NUMBERS

Grant #: FO8630-98-1-1004  
JON: 25020727 PE:62602F  
PR:2502  
TA:07  
WU:27

6. AUTHOR(S) Michael L. Stokes

7. PERFORMING ORGANIZATION NAME(S) AND ADDRESS(ES)

Mississippi State University  
Engineering Research Center  
P.O. Box 6810  
Mississippi State, MS 39762-9627

8. PERFORMING ORGANIZATION REPORT  
NUMBER

9. SPONSORING/MONITORING AGENCY NAME(S) AND ADDRESS(ES) (Program Mgr Name & Ph #)

USAF Research Laboratory  
Computational Mechanics Branch (AFRL/MNAC)  
101 W. Eglin Blvd, Ste #337  
Eglin AFB, Florida 32542-6810

10. SPONSORING/MONITORING AGENCY  
REPORT NUMBER

AFRL-MN-EG-TR-2001-7023

Program Manager: Dr Kirk Vanden, 850-882-3124 (x3351)

11. SUPPLEMENTARY NOTES

Availability of this report is specified on the verso of front cover.

12a. DISTRIBUTION/AVAILABILITY STATEMENT

**DISTRIBUTION A.** Approved for public release; distribution unlimited.

12b. DISTRIBUTION CODE

13. ABSTRACT:

In this report we describe the work in developing Eulerian upwind one-dimensional and two-dimensional numerical models for shock impact problems on unstructured grids, as well as exact solutions of one-dimensional uniaxial strain problems used to validate the numerical solutions. This report contains some fundamental theory used to derive the working equations, as well as examples used to illustrate the various solutions.

14. SUBJECT TERM unstructured hydrocode finite-volume elastic plastic impact

15. NUMBER OF PAGES  
81

16. PRICE CODE

17. SECURITY CLASSIFICATION OF  
REPORT  
UNCLASSIFIED

18. SECURITY CLASSIFICATION  
OF THIS PAGE  
UNCLASSIFIED

19. SECURITY CLASSIFICATION  
OF ABSTRACT  
UNCLASSIFIED

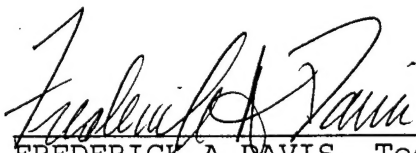
20. LIMITATION OF ABSTRACT  
SAR

## NOTICE

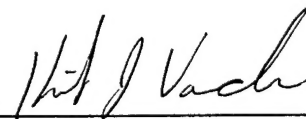
When Government drawings, specifications, or other data are used for any purpose other than in connection with a definitely Government-related procurement, the United States Government incurs no responsibility or any obligation whatsoever. The fact that the Government may have formulated or in any way supplied the said drawings, specifications, or other data, is not to be regarded by implication, or otherwise in any manner construed, as licensing the holder, or any other person or corporation; or as conveying any rights or permission to manufacture, use, or sell any patented invention that may in any way be related thereto.

This technical report is releasable to the National Technical Information Services (NTIS). At NTIS it will be available to the general public, including foreign nations.

This technical report has been reviewed and is approved for publication.



FREDERICK A DAVIS, Technical Director  
Assessment and Demonstrations Division



Dr Kirk Vanden  
Program Manager

If your address has changed, if you wish to be removed from our mailing list, or if your organization no longer employs the addressee, please notify AFRL/MNAC, Eglin AFB FL 32542-6810, to help us maintain a current mailing list.

Do not return copies of this report unless contractual obligations or notice on a specific document requires that it be returned.

# Contents

<b>1</b>	<b>Introduction</b>	<b>5</b>
<b>2</b>	<b>One-Dimensional Considerations</b>	<b>7</b>
2.1	Theoretical Aspects . . . . .	7
2.1.1	Equations of Motion . . . . .	7
2.1.2	Uniaxial Strain . . . . .	9
2.1.3	Two-wave response using the Mie-Grueneisen Equation of State. . . . .	29
2.1.4	Single-wave plastic response using the Mie-Grueneisen Equation of State. . . . .	32
2.1.5	The Equation of State . . . . .	32
2.2	Numerical Aspects . . . . .	34
2.2.1	Integration Scheme for the Conservation Equations . . . . .	34
2.2.2	Flux Evaluation . . . . .	37
2.2.3	Eigenvalue Calculation . . . . .	39
2.2.4	Integration of the Constitutive Equations . . . . .	40
2.2.5	A Turning Algorithm . . . . .	41
2.3	Numerical Results . . . . .	42
2.3.1	Hydrostatic Test Case . . . . .	43
2.3.2	Elastic Solution using the Experimental Hugoniot. . . . .	43
2.3.3	Elastic Solution using the Mie-Grueneisen Equation of State . . . . .	43
2.3.4	Two-Wave Solution Using the Mie-Grueneisen Equation of State. . . . .	44
2.3.5	Single-Wave Plastic Solution using the Mie-Grueneisen Equation of State. . . . .	45
<b>3</b>	<b>Two-Dimensional Considerations</b>	<b>47</b>
3.1	Conservation Equations . . . . .	47
3.2	Constitutive Equations . . . . .	48
3.3	Integration of the Conservation Equations . . . . .	48
3.4	Integration of the Constitutive Equations . . . . .	50
3.5	Results for Two-Dimensional Plane Strain . . . . .	50
<b>4</b>	<b>Conclusion</b>	<b>52</b>
<b>5</b>	<b>Recommendations</b>	<b>53</b>
<b>6</b>	<b>Additional Figures</b>	<b>54</b>

# List of Figures

2.1	Normal Shock Terminology. . . . .	13
2.2	Single shock wave impact configuration. . . . .	14
2.3	Single shock wave impact configuration for the elastic response. . . . .	18
2.4	Figure illustrating the two-wave Plastic Solution. . . . .	25
2.5	Figure illustrating the "Turning Method" . . . . .	46
3.1	The control volume using a dual medium grid. . . . .	49
6.1	Pressure for hydrostatic test case. . . . .	55
6.2	Density for hydrostatic test case. . . . .	56
6.3	Energy for hydrostatic test case. . . . .	57
6.4	Pressure for elastic test case using the Experimental Hugoniot. . . . .	58
6.5	Density for elastic test case using the Experimental Hugoniot. . . . .	59
6.6	Energy for elastic test case using the Experimental Hugoniot. . . . .	60
6.7	Deviatoric Stress for elastic test case using the Experimental Hugoniot. . . . .	61
6.8	Pressure for elastic test case using the Mie-Grueneisen equation of state. . . . .	62
6.9	Density for elastic test case using the Mie-Grueneisen equation of state. . . . .	63
6.10	Energy for elastic test case using the Mie-Grueneisen equation of state. . . . .	64
6.11	Deviatoric stress for elastic test case using the Mie-Grueneisen equation of state. . . . .	65
6.12	Pressure for two-wave test case using the Mie-Grueneisen equation of state. . . . .	66
6.13	Density for two-wave test case using the Mie-Grueneisen equation of state. . . . .	67
6.14	Energy for two-wave test case using the Mie-Grueneisen equation of state. . . . .	68
6.15	Deviatoric stress for two-wave test case using the Mie-Grueneisen equation of state. . . . .	69
6.16	Pressure for single-wave test case using the Mie-Grueneisen equation of state. . . . .	70
6.17	Density for single-wave test case using the Mie-Grueneisen equation of state. . . . .	71
6.18	Energy for single-wave test case using the Mie-Grueneisen equation of state. . . . .	72
6.19	Deviatoric stress for single-wave test case using the Mie-Grueneisen equation of state. . . . .	73
6.20	Pressure for impact of Copper Bar at 1000 m/s. . . . .	74
6.21	Initial Configuration of notched bar. . . . .	75
6.22	Deformed Configuration of notched bar with Pressure. . . . .	76

# List of Tables

2.1	Material properties used in the example problems. . . . .	17
2.2	Results of the numerical procedure for the shock impact problem for state 2 using the Mie-Grueneisen Equation of State. . . . .	24
2.3	Result of numerical procedure at states 2 and 3 using the Mie-Grueneisen equation of state for the two wave problem. . . . .	32
2.4	Result of numerical procedure for states 2 and 3 using the Mie-Grueneisen equation of state for the single plastic wave problem. . . . .	33
2.5	Exact vs. Computed Results for Hydrostatic case(State 2). . . . .	43
2.6	Exact vs. Computed Results for Elastic case(State 2) using the Experimental Hugoniot. . . .	44
2.7	Exact vs. Computed Results for Elastic case(State 2) using the Mie-Grueneisen Equation of State. . . . .	44
2.8	Exact vs. Computed Results for the Two-wave Shock using the Mie-Grueneison Equation of State. . . . .	44
2.9	Exact vs. Computed Results for the Plastic Single-Wave response using the Mie-Grueneisen Equation of State. . . . .	45

## NOMENCLATURE

$c_0$	=	constant in the equation of state
$e$	=	internal energy per unit mass
$e_T$	=	total internal energy per unit mass
$\Delta\phi$	=	variation of $\phi$ in space
$\delta\phi$	=	variation of $\phi$ in time
$D_{ij}$	=	deformation rate tensor
$D'_{ij}$	=	deviator of the deformation rate tensor
$\bar{\epsilon}$	=	plastic strain
$\mathbf{f}, \mathbf{f}_i$	=	flux vector
$\mathcal{F}$	=	flux function
$G$	=	bulk Shear Modulus
$\Gamma_0$	=	plastic material constant
$H_0$	=	y-intercept of the plastic yield function
$H'(\bar{\epsilon})$	=	slope of plastic yield function
$\Omega_{ij}$	=	spin tensor
$p$	=	hydrostatic pressure
$\mathbf{Q}_j$	=	heat flux
$\mathbf{q}$	=	velocity vector(u,v,w)
$\rho$	=	density
$\rho_0$	=	pre-shock density
$s$	=	constant in the equation of state
$s_{ij}$	=	deviator stress tensor
$\sigma_{ij}$	=	stress tensor
$\bar{\sigma}$	=	equivalent or von Mises stress
$S(\mathbf{U})$	=	source terms
$S_x$	=	deviatoric stress in x direction
$S_y$	=	deviatoric stress in y direction
$S_{xy}$	=	deviatoric shear stress in xy plane
$\mathbf{U}$	=	vector of conserved variables
$U_s$	=	shock speed
$\mathbf{v}_j$	=	tensor velocity
$V$	=	specific density
$V_0$	=	pre-shock specific density

# Chapter 1

## Introduction

The US military has known that certain munitions will suffer premature ignition if the internal pressure wave generated from a mechanical insult is of sufficiently large magnitude. Current numerical solutions often do not provide adequate estimates of the pressure magnitude due to the application of artificial viscosity needed to maintain the stability of the numerical scheme. Other inaccuracies may be inadequate resolution of grid points in regions through which shocks propagate, and inaccuracies due to a massive skewing of the grid subject to large deformations. A similar example is found in the impact of high-speed munitions designed to penetrate concrete bunkers and explode at depth below the surface. In both examples it is necessary to properly capture the magnitude of the pressure wave created by impact induced shocks.

One approach to accurately capture this phenomena is to cast the equations of motion in a conservative Eulerian form. This approach has several advantages;

- Mass continuity, momentum, and energy are strictly conserved. Other formulations such as the Arbitrary Lagrangian Eulerian or ALE approach maintain mass, but the conservation of energy is not strictly conserved.
- The Eulerian form can be cast in multiple coordinate frames including the material frame where the viewpoint of an observer is coincident with the particle velocity of the material, or from a reference frame at a fixed location, or from an arbitrary reference location including one which is a function of time. This freedom allows a great deal of flexibility in dealing with the quality of the discretization during extensive deformation of the solution.

However, despite obvious advantages of this approach, the Eulerian form has not been embraced by a majority of researchers.<sup>1</sup> The classical methods of integrating these equations such as the Lax-Wendroff class of schemes are highly oscillatory in the neighborhood of discontinuities without special treatment. Fortunately, much work has been done in the Computational Fluid Dynamics community which can be re-invented for the equations of hydrodynamics. One example is the notion of “upwind” schemes which provide essentially non-oscillatory results with sharply defined shock fronts. The current research extends the upwind approach to accommodate grid advection during the integration phase of the solution while maintaining at least second order accuracy in both time and space.

This document describes the work in developing one-dimensional and two-dimensional numerical models for shock impact problems, as well as exact solutions of one-dimensional uniaxial strain problems used to

---

<sup>1</sup>See reference [1] for a survey on these techniques



validate the numerical solutions. It contains some fundamental theory used to derive the working equations, as well as examples used to illustrate the various solutions. The numerical examples are illustrated in Chapter 6 using screen captures of the working programs to illustrate the behavior of the numerical codes.

## Chapter 2

# One-Dimensional Considerations

This chapter develops the theory for exact and numerical procedures of the uniaxial strain problem with examples used to illustrate the concepts.

### 2.1 Theoretical Aspects

The contents of this section are derived from a number of existing sources including [2],[3],[4], and [5], many of which are out of current publication. As the result, some of the developmental material is presented to provide a reasonably complete treatise on the topic. Much of the theory was provided and explained from unpublished notes authored by Dr. Davy Belk of Eglin AFB. The remaining material was developed by the author as necessary to complete the requirements of the contract.

#### 2.1.1 Equations of Motion

The equations of motion are comprised of a set of equations which provide for the conservation of mass, momentum, and energy along with a set of non-linear constitutive equations which define the material derivatives of stress and strain. The equations are closed with an appropriate equation of state relating pressure to internal energy, velocity, stress, and strain. The fully three-dimensional form of the equations will be presented, then reduced to one dimension using the assumption of uniaxial strain with elastic/plastic deformation.

#### Conservation Equations

The conservation law equations are identical for both solid and fluid mediums. The only variation is in the form of the stress tensor and any source terms that may be present. These equations in divergence form are

$$\frac{\partial \rho}{\partial t} + (\rho v_j)_{,j} = 0 \quad (2.1)$$

$$\frac{\partial v_i}{\partial t} + (\rho v_i v_j - \sigma_{ji})_{,j} = \rho f_i \quad (2.2)$$

$$\frac{\partial(\rho e_T)}{\partial t} + (\rho e_T v_j - v_k \sigma_{jk} + \mathbf{Q}_j)_{,j} = \rho v_k f_k \quad (2.3)$$

In Cartesian components, the stress tensor  $\sigma_{ij}$  can be represented as the sum of the deviator stress  $s_{ij}$  and the hydrostatic stress components as

$$\sigma_{ij} = s_{ij} - p\delta_{ij} \quad (2.4)$$

where the pressure  $p$  is defined as positive in compression to match our usual idea of pressure which is related to the stress tensor by

$$-p = \frac{\sigma_{kk}}{3} \quad (2.5)$$

This quantity, the negative of the mean normal stress, is not always equivalent to thermodynamic pressure, but will be considered as such in this context.

Defining  $D_{ij}$  as the classic deformation rate tensor and  $D'_{ij}$  as the deviator of the deformation rate tensor

$$D_{ij} = \frac{1}{2}(v_{i,j} + v_{j,i}) \quad (2.6)$$

$$D'_{ij} = D_{ij} - \frac{1}{3}D_{kk}\delta_{ij} \quad (2.7)$$

The Prandtl-Reuss expressions relating deviator stress rate (corrected for material frame indifference) to plastic strain rate are given by

$$\frac{ds_{ij}}{dt} = \Omega_{ik}s_{kj} - s_{ik}\Omega_{kj} + 2G \left( D'_{ij} - \frac{3}{2}\beta \frac{s_{ij}s_{mn}}{\sigma^2} D'_{mn} \right) \quad (2.8)$$

$$\frac{d\bar{\epsilon}}{dt} = \beta \frac{s_{ij}}{\sigma} D'_{ij} \quad (2.9)$$

where  $\beta$  is defined as

$$\beta = \frac{k}{1 + \frac{H'(\bar{\epsilon})}{3G}} \quad \text{where, } \begin{cases} k \rightarrow 1 & \text{plastic loading} \\ k \rightarrow 0 & \text{Otherwise} \end{cases} \quad (2.10)$$

and the spin tensor  $\Omega_{ij}$  is defined as

$$\Omega_{ij} = \frac{1}{2}(v_{i,j} - v_{j,i}) \quad (2.11)$$

The set of conservation laws Eq.[2.1- 2.3] and the constitutive equations Eqs.[2.8 - 2.9] when combined with an equation of state (Section 2.1.5) provide a complete description of the equations of motion for an elastic or plastic medium.

### 2.1.2 Uniaxial Strain

To reduce the constitutive Eqs.[2.8][2.9] for the case of uniaxial strain, it will be assumed that no shear stresses can exist and that deformation is only allowed in the direction of motion. For this case the stress tensor is not one-dimensional, but rather assumes symmetry in the transverse direction. For this case, the stress tensor is given by

$$[\sigma_{ij}] = \begin{bmatrix} \sigma_x & 0 & 0 \\ 0 & \sigma_y & 0 \\ 0 & 0 & \sigma_y \end{bmatrix} \quad (2.12)$$

The negative of the mean stress from Eq.2.5 is given by

$$p = -\frac{1}{3}(\sigma_x + 2\sigma_y) \quad (2.13)$$

The stress deviator components are calculated by solving Eq.2.4 for  $s_{ij}$

$$[s_{ij}] = \begin{bmatrix} \frac{2}{3}(\sigma_x - \sigma_y) & 0 & 0 \\ 0 & -\frac{1}{3}(\sigma_x - \sigma_y) & 0 \\ 0 & 0 & -\frac{1}{3}(\sigma_x - \sigma_y) \end{bmatrix} \quad (2.14a)$$

$$= \begin{bmatrix} s_x & 0 & 0 \\ 0 & -\frac{1}{2}s_x & 0 \\ 0 & 0 & -\frac{1}{2}s_x \end{bmatrix} \quad (2.14b)$$

Similarly, the deviator of the deformation tensor is given by

$$[D'_{ij}] = \begin{bmatrix} \frac{2}{3} \frac{\partial u}{\partial x} & 0 & 0 \\ 0 & -\frac{1}{3} \frac{\partial u}{\partial x} & 0 \\ 0 & 0 & -\frac{1}{3} \frac{\partial u}{\partial x} \end{bmatrix} \quad (2.15)$$

The equivalent or von Mises stress  $\bar{\sigma}$  is defined as

$$\bar{\sigma} \equiv \left( \frac{3}{2} s_{ij} s_{ij} \right)^{\frac{1}{2}} = \frac{3}{2} |s_x| = |\sigma_x - \sigma_y| \quad (2.16)$$

Plastic loading occurs when the equivalent stress reaches the yield function  $H'(\bar{\epsilon})$

$$\bar{\sigma} = \frac{2}{3} |s_x| = H'(\bar{\epsilon}) \quad (2.17)$$

and

$$\frac{\partial u}{\partial x} s_x > 0 \quad (2.18)$$

If the two conditions specified in Eqs.[2.17] [2.18] are satisfied, then  $k$  in Eq.[2.10] is 1, corresponding to plastic deformation, otherwise  $k = \beta = 0$  and the strain rate given by Eq.[2.9] is 0.

With the previous definitions of stress and strain, the conservation and the constitutive equations for uniaxial strain reduce to

$$\frac{\partial \rho}{\partial t} + \frac{\partial(\rho u)}{\partial x} = 0 \quad (2.19a)$$

$$\frac{\partial(\rho u)}{\partial t} + \frac{\partial(\rho u^2 + P - S_x)}{\partial x} = 0 \quad (2.19b)$$

$$\frac{\partial(\rho e_T)}{\partial t} + \frac{\partial[u(\rho e_T + P - S_x)]}{\partial x} = 0 \quad (2.19c)$$

$$\frac{dS_x}{dt} = (1 - \beta) \frac{4}{3} G \frac{\partial u}{\partial x} \quad (2.19d)$$

$$\frac{d\bar{\epsilon}}{dt} = \beta \frac{2}{3} \left| \frac{\partial u}{\partial x} \right| \quad (2.19e)$$

Note that the coupling of  $\bar{\epsilon}$  in Eqs.[2.19a-2.19d] is due to the fact that  $\beta$  (Eq.[2.10]) is a function of  $H'(\bar{\epsilon})$  which influences the stress rate in Eq.[2.19d]. However, for purely plastic deformation where  $H'(\bar{\epsilon})$  is a constant,  $\beta$  will be a constant and Eq.[2.19e] decouples from the equation set.

Part of the early research work was in casting the advection Eqs.[2.19d,2.19e] in a form where the entire equation set could be solved as set of partial differential equations. However, the advection equations would have to be manipulated such that the left-hand side was in a divergence form with all *remaining terms* treated as source terms on the right-hand side. The advantage of this scheme would be a higher level of coupling between the five equations since the eigenvalues of the coupled system would have the contributions of the constitutive equations. There is however no unique method for determining which terms should appear on the left-hand side, though this issue has been a point of research.

As following [6], consider a generalized advection equation of the form

$$\phi_t + u\phi_x = 0 \quad (2.20)$$

which when multiplied by  $\rho$  and combined with the continuity equation [2.19a] can be expressed in the divergence form

$$(\rho\phi)_t + (\rho u\phi)_x = 0 \quad (2.21)$$

Note that Eqs.[2.19d,2.19e] can be put in this form for the special cases of  $\beta = 1$  and  $\beta = 0$ , respectively. The well known jump condition for Eq.[2.21] is given by

$$\rho_L \phi_L (u_L - U_s) = \rho_R \phi_R (u_R - U_s) \quad (2.22)$$

where  $U_s$  is the speed of the discontinuity, and the R and L subscripts refer to the right and left states, respectively. If the jump condition for continuity given by

$$\rho_L (u_L - U_s) = \rho_R (u_R - U_s) \quad (2.23)$$

divides Eq.[2.22], then  $\phi_L = \phi_R$  indicating that  $\phi$  would be continuous across the shock. Fedkiw[6] concludes that if  $\phi$  is discontinuous across a shock, then Eq.[2.21] would be an inappropriate form for generalized advection equations.

While the development of the argument is correct, it is not obvious that the conclusion is definitive for the current application. It should be obvious that his argument holds only in the case where the additional equations are part of the weak solution resulting in jumps relations, which for the current application is not applicable. Additionally, his arguments are only valid for equations which are truly in a divergence form, which again does not match the current case.

Another approach to determine an appropriate divergence form of the constitutive equations was to consider the eigen properties of a candidate form to determine if the equations remained hyperbolic. Most of the variations studied had singular transformation matrices, resulting in an incompatible form. One form which did not exhibit this property was the form given by Eq.[2.21]. However, the eigenvalues for this form were the same as for the conservation equations alone, thus this form would be of no additional advantage in a flux based algorithm.

The upshot of the current work is that solving Eqs.[2.19d,2.19e] with the conservation equations as a set of partial differential equations is not recommended. It will be shown that the exact solution of the conserved variables is dependent only on the initial state of stress, being independent of the derivatives of  $S_x$  or  $\bar{\epsilon}$ . This provides a natural decoupling of the constitutive equations which should be mimicked by the numerical procedure. From a philosophical standpoint, attempts to pose advection equations in a contrived conservative form could create unphysical artifacts in the solution of the equations.

## Exact Shock Solutions

The “genuine solution” of the partial differential equation in the general form

$$\frac{\partial \rho}{\partial t} + \frac{\partial Q(\rho)}{\partial x} = 0 \quad (2.24)$$

is strictly only valid where the derivatives are defined. Therefore, a discontinuous solution cannot be said to be *genuine* when  $\rho$  or  $Q(\rho)$  are discontinuous. The concept of weak solutions is used to extend the solution set to include discontinuities. The solution set is represented by

$$-U_s[\rho] + [Q] = 0 \quad (2.25)$$

where the square brackets are used to indicate the jump across the discontinuity, i.e.

$$[\rho] = \rho_2 - \rho_1 \quad (2.26)$$

$$[Q] = Q_2 - Q_1 \quad (2.27)$$

and  $U_s$  is the shock velocity given by

$$U_s = \frac{\frac{dx}{ds}}{\frac{dt}{ds}} = \frac{dx}{dt} \quad (2.28)$$

The general solution given by Eq.[2.25] as applied to the set of conservation equations Eq.[2.19a-2.19c] without heating or other body forces is given by

$$U_s[\rho] = [\rho v] \quad (2.29)$$

$$U_s[\rho v] = [\rho v^2] - [\sigma] \quad (2.30)$$

$$U_s \left[ \rho \left( e + \frac{1}{2} v^2 \right) \right] = \left[ \rho \left( e + \frac{1}{2} v^2 \right) v \right] - [\sigma v] \quad (2.31)$$

These equations are the Rankine-Hugoniot Equations for uniaxial strain. To develop a general solution framework for specific problems, a special case is derived where the reference frame  $U_s = 0$  resulting in

$$\rho_1 v_1 = \rho_2 v_2 \quad (2.32)$$

$$\rho_1 v_1^2 - \sigma_1 = \rho_2 v_2^2 - \sigma_2 \quad (2.33)$$

$$\rho_1 \left( e_1 + \frac{1}{2} v_1^2 \right) v_1 - \sigma_1 v_1 = \rho_2 \left( e_2 + \frac{1}{2} v_2^2 \right) v_2 - \sigma_2 v_2 \quad (2.34)$$

where  $v_1$  and  $v_2$  are velocities relative to the stationary shock. Substituting Eq.[2.32] into Eq.[2.34] results in

$$e_2 - e_1 = \frac{1}{2} (v_1^2 - v_2^2) - \frac{\sigma_1}{\rho_1} + \frac{\sigma_2}{\rho_2} \quad (2.35)$$

Using Eq.[2.33] to eliminate velocities the above equation can be written as

$$e_2 - e_1 = \frac{1}{2} (\sigma_1 + \sigma_2) (V_2 - V_1) \quad (2.36)$$

This equation is often referred to as the Hugoniot equation. Note that the expression is independent of coordinate system and involves only thermodynamic variables. Another useful expression is found by solving for  $U_s$  in Eq.[2.29] and substituting the result into Eq.[2.30] resulting in

$$(v_1 - v_2)^2 = (\sigma_2 - \sigma_1) (V_2 - V_1) \quad (2.37)$$

For a normal shock (Figure.2.1) propagating with unknown velocity  $U_s$  into condition 2, there are 3 Rankine-Hugoniot equations, but there are five unknowns, i.e.  $v_2, p_2, e_2, \rho_2$ , and  $U_s$ . In order to close the system, two more conditions must be supplied. The conditions are typically an equation of state relating pressure, energy, and density, together with any one of the state variables downstream of the shock. With this information, all other unknowns at state 2 can be determined.

The shock problem is defined as the impact of two infinite length bars, which in general, may be different materials, and impact one another at a contact discontinuity. Uniaxial strain will only be considered, thus the bars are confined in such a way as to prohibit lateral or non-axial deformation.

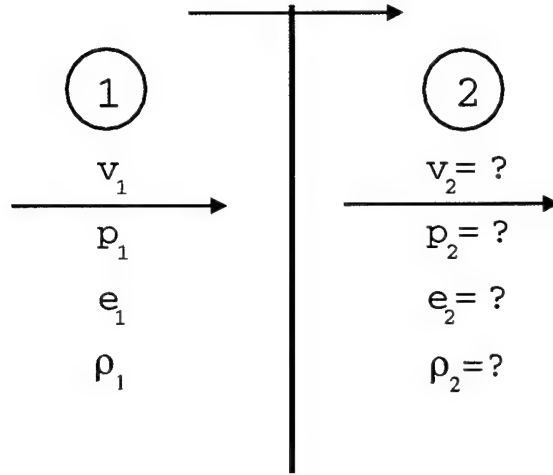


Figure 2.1: Normal Shock Terminology.

### Experimental Hugoniot

Sometimes a Hugoniot curve is erroneously referred to as an “equation of state” for the material. An equation of state is an entire surface in  $(P, V, e)$  space such that given arbitrary values of two of the parameters, the third can be determined. The Hugoniot is a single curve on this surface. By assuming a particular form of the equation of state, an experimentally determined Hugoniot is often used to determine coefficient values that are then applied off the Hugoniot. The misuse of the “equation of state” terminology is that in the absence of an equation of state, any condition involving one or more of the unknown values can be used to make the system determinate as long as the condition is independent of the jump conditions. This condition is then used as a replacement for the equation of state for solving shock problems, but it should not be mistaken as equivalent to an equation of state.

One such condition is a linear relation between shock speed  $U_s$  and particle velocity  $v$  given by

$$U_s = c_0 + sv \quad (2.38)$$

where the reference frame is such that the initial particle velocity is zero and the shock speed is positive. The coefficients  $c_0$  and  $s$  are determined experimentally where  $c_0$  is close to the linear longitudinal wave speed. For the case as shown in Figure [2.1] where the shock speed is shown positive to the right, then Eq.[2.38] is rewritten as

$$U_s - v_2 = c_0 + s(v_1 - v_2) \quad (2.39)$$

This equation is called the right-running wave. If the wave is propagating in the negative direction with respect to the material, then the formula would read

$$U_s - v_1 = -c_0 + s(v_2 - v_1) \quad (2.40)$$



This equation is called the left-running wave. One of these empirical relations Eq.[2.39,2.40], as appropriate, can be used to analytically represent the Hugoniot curve and will be referred to as the Experimental Hugoniot.

### Hydrostatic Solution

For the hydrostatic case, the deviatoric stress is set to zero. The impact of two bars will initiate a single shock wave through each material as illustrated in Figure [2.2]. The left material will contain the reflected shock with velocity  $U_{rs}$  and the right material will contain the transmitted shock with velocity  $U_{ts}$ . At the impact point between states 2 and 3, a contact discontinuity exists with velocity  $U_c$ , therefore, the materials are not allowed to mix.

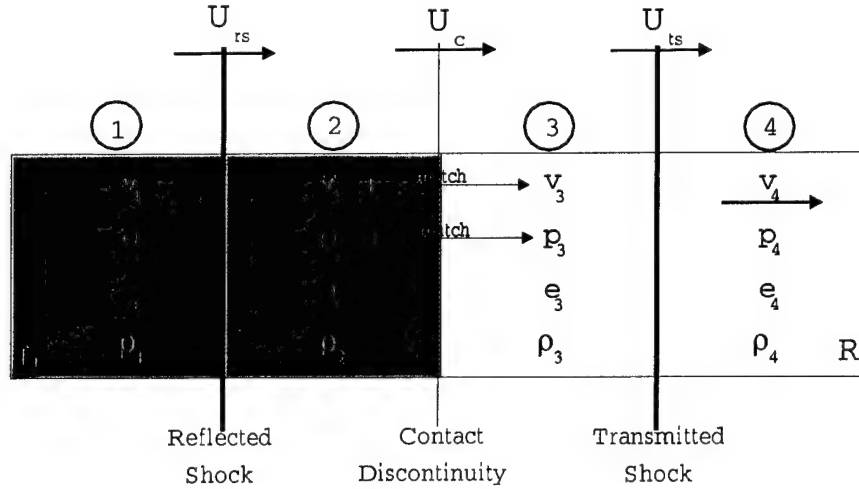


Figure 2.2: Single shock wave impact configuration.

To determine which properties must be conserved, consider the Rankine-Hugoniot Equations [2.29] through [2.31] as applied between states 2 and 3 as illustrated in Figure [2.2]. Applying Eq.[2.29] results in

$$U_s(\rho_2 - \rho_3) = U_c(\rho_2 - \rho_3) \quad (2.41)$$

indicating (1) that  $U_s = U_c$ , or simply that the speed of the discontinuity must equal the local particle velocity on either side of the interface, i.e.  $U_c = v_2 = v_3$ , and (2) that a jump in density may exist at the contact discontinuity. Applying the momentum Eq.[2.30] across the contact discontinuity results in  $\sigma_2 = \sigma_3$ , or simply that the normal stress must be continuous across the contact discontinuity. For the hydrostatic case, this requires  $p_2 = p_3$ . Applying the energy Eq.[2.31] across the interface indicates that a jump in energy may exist at the contact discontinuity.

For the configuration shown in Fig.[2.2], there are eleven unknowns including  $U_{rs}$ ,  $v_2$ ,  $p_2$ ,  $e_2$ , and  $\rho_2$  from the left material,  $U_{ts}$ ,  $v_3$ ,  $p_3$ ,  $e_3$ , and  $\rho_3$  from the right material, and  $U_c$  from the contact discontinuity. From these, three are duplicates with  $v_2 = v_3 = U_c$ , and  $p_2 = p_3$ , therefore, in total there are eight independent unknowns. For the left material there are three Rankine-Hugoniot jump relations and one Experimental Hugoniot expression relating the jump conditions between states 1 and 2. Similarly, there are

four additional conditions from the right material relating the jump conditions between states 3 and 4. Since there are eight equations and eight unknowns, the problem is well-posed.

The solution procedure begins by finding the speed of the contact discontinuity. This provides the velocity at states 2 and 3 by satisfying continuity in the normal stress at the contact discontinuity. With this information, the jump conditions will be analyzed for the remainder of the properties at states 2 and 3.

The density at state 2 is expressed using Eq.[2.29] as a function of the respective shock speed and velocity jump where

$$\rho_2 = \rho_1 \frac{U_{rs} - v_1}{U_{rs} - v_2} \quad (2.42)$$

and similarly for state 3

$$\rho_3 = \rho_4 \frac{U_{ts} - v_4}{U_{ts} - v_3} \quad (2.43)$$

Solving the momentum equation Eq.[2.30] between states 1 and 2 for normal stress and substituting Eq.[2.42] results in

$$\sigma_2 = \sigma_1 + (U_{rs} - v_1)(v_1 - v_2)\rho_1 \quad (2.44)$$

Similarly between states 3 and 4 we have

$$\sigma_3 = \sigma_4 + (U_{ts} - v_4)(v_4 - v_3)\rho_4 \quad (2.45)$$

Since the normal stress must be continuous across the contact discontinuity, Eqs.[2.44,2.45] are equated and simplified by substituting expressions for the shock speeds from Eqs.[2.39,2.40] to give a quadratic expression in terms of  $U_c$  where

$$A_2 U_c^2 + A_1 U_c + A_0 = 0 \quad (2.46)$$

The coefficients of the polynomial are defined as

$$A_2 = s^R \rho_4 - s^L \rho_1 \quad (2.47)$$

$$A_1 = \rho_1 (c_0^L + 2v_1 s^L) + \rho_4 (c_0^R - 2v_4 s^R) \quad (2.48)$$

$$A_0 = \rho_4 v_4 (-c_0^R + s^R v_4) - \rho_1 v_1 (c_0^L + s^L v_1) + \sigma_1 - \sigma_4 \quad (2.49)$$

where the superscripts R and L refer to the right and left materials. For  $A_2 = 0$ ,

$$U_c = -\frac{A_0}{A_1} \quad (2.50)$$

otherwise, the solution is given by the negative root of the quadratic formula

$$U_c = \frac{-A_1 - \sqrt{A_1^2 - 4A_0A_2}}{2A_2} \quad (2.51)$$

where the negative root is required such at  $v_1 > U_c > v_4$ . For the special case where the material and thermodynamic properties are identical at states 1 and 4, Eq.[2.50] reduces to

$$U_c = \frac{1}{2}(v_1 + v_4) \quad (2.52)$$

The shock speeds can be found by applying Eqs.[2.40] and [2.39] where

$$U_{rs} = v_1 - c_0^L + s^L(v_2 - v_1) \quad (2.53)$$

$$U_{ts} = v_4 + c_0^R + s^R(v_3 - v_4) \quad (2.54)$$

The densities can be calculated from Eqs.[2.42] and [2.43], and the pressures using Eqs.[2.44] and [2.45] realizing that  $p_2 = -\sigma_2$  and  $p_3 = -\sigma_3$ . Energies can be calculated from Eq.[2.36] where

$$e_2 = e_1 + \frac{1}{2}(p_1 + p_2)(V_1 - V_2) \quad (2.55)$$

$$e_3 = e_4 + \frac{1}{2}(p_3 + p_4)(V_4 - V_3) \quad (2.56)$$

Note that this solution did not require the use of an explicit equation of state. However, it can be shown that the Mie-Grueneisen Equation of State if applied to the hydrostatic case would provide the same pressure since the solution stays on the same Hugoniot line. Also, although the energy equation was not used, it can be shown that the solution does satisfy the conservation of energy across the shock.

#### **EXAMPLE: Hydrostatic Response using the Experimental Hugoniot.**

Consider two bars impacting one another with identical material properties as shown in Table [2.1]. The left bar has a velocity of  $v_1 = 100 \text{ m/s}$  and the right bar is moving at  $v_4 = -100 \text{ m/s}$ . The density of both bars are  $\rho_1 = \rho_4 = 8930 \frac{\text{kg}}{\text{m}^3}$ . The pressure and energy of both bars are zero. The problem is to find the states 2 and 3 as shown in Fig. [2.2] assuming a hydrostatic response.

Using Eq.[2.52] to calculate the velocity of the contact discontinuity

$$U_c = 0.5(100.0 + -100.0) = 0.0 \text{ m/s} \quad (2.57)$$

Using Eqs.[2.53] and [2.54] to calculate the shock speeds

$$U_{rs} = 100.0 - 3940.0 + 1.49(0.0 - 100.0) = -3989.0 \text{ m/s}$$

$$U_{ts} = -100.0 + 3940.0 + 1.49(0.0 - -100.0) = 3989.0 \text{ m/s}$$

Using Eqs.[2.42] and [2.43] used to calculate the densities

Table 2.1: Material properties used in the example problems.

$c_0$	$=$	$3940 \text{ m/s}$
$\rho_0$	$=$	$8930 \text{ kg/m}^3$
$\Gamma$	$=$	$2.0$
$s$	$=$	$1.49$
$H_0$	$=$	$300 \text{ MPa}$
$H'$	$=$	$30 \text{ MPa}$
$E$	$=$	$121.9 \text{ GPa}$
$G$	$=$	$45 \text{ GPa}$

$$\rho_2 = 8930 \frac{(-3989.0 - 100.0)}{(-3989.0 - 0.0)} = 9153.865634 \text{ kg/m}^3$$

$$\rho_3 = 8930 \frac{(3989.0 - -100.0)}{(3989.00.0)} = 9153.865634 \text{ kg/m}^3$$

The normal stresses can be calculated from Eqs.[2.44] and [2.45] as follows

$$\sigma_2 = 0 + (-3989.0 - 100.0)(100.0 - 0.0) \cdot 8930.0 = -3.651477 \text{ GPa}$$

$$\sigma_3 = 0 + (3989.0 - -100.0)(-100.0 - 0.0) \cdot 8930.0 = -3.651477 \text{ GPa}$$

Since there is no deviatoric stress for the hydrostatic case, the pressures at states 2 and 3 are simply the negative of the normal stresses, or

$$p_2 = -\sigma_2 = 3.651477 \text{ GPa}$$

$$p_3 = -\sigma_3 = 3.651477 \text{ MPa}$$

The energies are calculated using Eqs.[2.55,2.56] as follows

$$e_2 = 0.0 + 0.5 \cdot \left( 0.0 + 3.651477e^9 \right) \left( \frac{1.0}{8930.0} - \frac{1.0}{9153.865634} \right) = 5000.0 \text{ J/Kg}$$

$$e_3 = 0.0 + 0.5 \cdot \left( 3.651477e^9 + 0.0 \right) \left( \frac{1.0}{8930.0} - \frac{1.0}{9153.865634} \right) = 5000.0 \text{ J/Kg}$$

## Elastic Solution using the Experimental Hugoniot

The constants  $c$  and  $s$  given for the Experimental Hugoniot will not be applicable for impact velocities in the elastic range, and therefore will not give results consistent with experiment<sup>1</sup>. However, it is instructive to develop these relationships for the reader as a progression of complexity both from the mathematical as well as science perspective. Hopefully the value in this approach will be appreciated in the current and following sections.

The elastic solution is similar to the hydrostatic solution in that an impact will generate a transmitted and reflected shock as shown in Figures [2.3]. However, unlike the hydrostatic case, deviatoric stress is produced and must be accounted for as a component of normal stress.

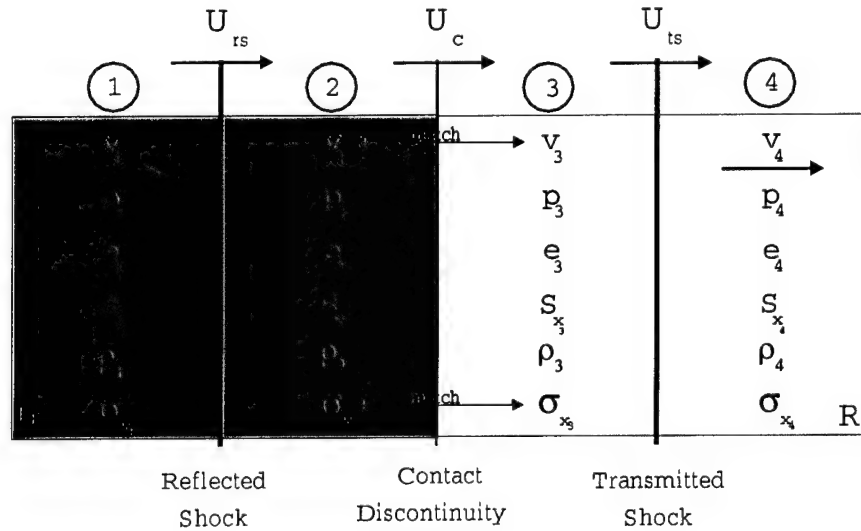


Figure 2.3: Single shock wave impact configuration for the elastic response.

There are fifteen unknowns which are  $U_{rs}$ ,  $\rho_2$ ,  $v_2$ ,  $p_2$ ,  $e_2$ ,  $S_{x_2}$ , and  $\sigma_2$  from the left material and  $U_{ts}$ ,  $\rho_3$ ,  $v_3$ ,  $p_3$ ,  $e_3$ ,  $S_{x_3}$ , and  $\sigma_3$  for the right material, and  $U_c$  from the contact discontinuity. From these three are duplicates with  $v_2 = v_3 = U_c$  and  $\sigma_2 = \sigma_3$ , leaving twelve unknowns. For the left material there are three Hugoniot-Rankine Equations, the Experimental Hugoniot,  $\sigma_2 = S_{x_2} - p_2$ , and  $S_x = S_x(\rho_2)$  that relates deviatoric stress to density resulting in six independent equations for the left material. Similarly, there are six equations for the right material or twelve total equations matching twelve unknowns. This forms a well-posed system.

The calculation of the contact discontinuity speed, the densities, the normal stresses, and the energies at states 2 and 3 are the same as calculated for the hydrostatic case (Section 2.1.2). To calculate the deviatoric stress, the assumption is made that the material response is elastic and that the Von Mises effective stress  $\bar{\sigma}$  must be below the yield surface, or

<sup>1</sup>the use of the Experimental Hugoniot will severely underpredict the shock speeds for an elastic shock. This statement also holds for the hydrostatic test case discussed in the previous section.

$$\frac{3}{2}|S_x| \leq \bar{\sigma} \quad (2.58)$$

Since the value of deviatoric stress is not known at this point, the procedure is to simply guess that the solution is elastic. If the guess is wrong then the elastic procedure will be abandoned for a plastic solution discussed later in the chapter.

The deviatoric stress is determined from Eq.[2.19d] cast in a differential form where

$$dS_x = \frac{4}{3}Gd\epsilon \quad (2.59)$$

where for an elastic response  $\beta = 0$  and  $\frac{\partial v}{\partial x} = \epsilon$ . Substituting the natural strain formulation  $d\epsilon = \frac{dl}{l}$  in the above equation and integrating from some initial state 0 results in

$$\int_{S_{x_0}}^{S_x} dS_x = \frac{4}{3}G \int_{l_0}^l \frac{dl}{l} \quad (2.60)$$

$$S_x = S_{x_0} + \frac{4}{3}G \ln \frac{l}{l_0} \quad (2.61)$$

For uniaxial strain, volumetric and longitudinal strain are identical, therefore,

$$\frac{l}{l_0} = \frac{V}{V_0} = \frac{\rho_0}{\rho} \quad (2.62)$$

Substituting this expression into Eq.[2.61] leaves

$$S_x = S_{x_0} + \frac{4}{3}G \ln \frac{\rho_0}{\rho} \quad (2.63)$$

Writing this expression between states 1 and 2 shown in Fig.[2.2] results in

$$S_{x_2} = S_{x_1} + \frac{4}{3}G^L \ln \frac{\rho_1}{\rho_2} \quad (2.64)$$

Similarly for state 3 the deviatoric stress is given by

$$S_{x_3} = S_{x_4} + \frac{4}{3}G^R \ln \frac{\rho_4}{\rho_3} \quad (2.65)$$

With deviatoric stress calculated and validated not to exceed the yield surface (Eq.[2.58]), the pressures can be calculated at states 2 and 3 by

$$p_2 = S_{x_2} - \sigma_2 \quad (2.66)$$

$$p_3 = S_{x_3} - \sigma_3 \quad (2.67)$$

The energies can now be calculated using Eq.[2.55] and all unknowns are defined.

**EXAMPLE: Elastic Response using the Experimental Hugoniot.**

The same configuration for the material properties and initial conditions will be used as in Section 2.1.2, except that the velocity at state 1 will be set to 10 m/s and the velocity at state 4 to -10 m/s so that the response will be elastic. Since the calculations are symmetric, the velocity of the contact discontinuity  $U_c$  will be zero. The shock speed as calculated from Eq.[2.53] is

$$U_{rs} = 10.0 - 3940.0 + 1.49(0.0 - 10.0) = -3944.9 \text{ m/s}$$

and the shock speed as calculated from Eq.[2.54] is

$$U_{ts} = -10.0 + 3940.0 + 1.49(0.0 - -10.0) = 3944.9 \text{ m/s}$$

The density for state 2 as calculated from Eq.[2.42] is

$$\rho_2 = 8930 \frac{(-3944.9 - 10.0)}{(-3944.9 - 0.0)} = 8952.637 \text{ kg/m}^3$$

The density for state 3 as calculated from Eq.[2.43] is

$$\rho_3 = 8930 \frac{(3944.9 - -40.0)}{(3944.9 - 0.0)} = 8952.637 \text{ kg/m}^3$$

The normal stress at state 2 as given by Eq.[2.44] is

$$\sigma_2 = 0.0 + (-3944.9 - 10.0)(10.0 - 0.0) \cdot 8930.0 = -353.1726 \text{ MPa}$$

The normal stress at state 3 as given by Eq.[2.45] is

$$\sigma_3 = 0.0 + (3944.9 - -10.0)(-10.0 - 0.0) \cdot 8930.0 = -353.1726 \text{ MPa}$$

The deviatoric stress at state 2 is given by Eqs.[2.64] as

$$S_{x_2} = 0 + \frac{4}{3} \cdot 45.0 \cdot 10^9 \ln \frac{8930.0}{8952.637} = -151.9038 \text{ MPa}$$

and the deviatoric stress at state 3 is given by [2.65] as

$$S_{x_3} = 0 + \frac{4}{3} \cdot 45.0 \cdot 10^9 \ln \frac{8930.0}{8952.637} = -151.9038 \text{ MPa}$$

The energy at state 2 as given by Eq.[2.36] is

$$e_2 = 0.0 + 0.5 \cdot \left( 0.0 + -353.1726e^6 \right) \left( \frac{1.0}{8952.637} - \frac{1.0}{8930.0} \right) = 50.00 \text{ J/Kg}$$

The pressure at state 2 is given by

$$p_2 = S_{x_2} - \sigma_2 = -151.9038e^6 - -353.1726e^6 = 201.2688 \text{ MPa}$$

and the pressure at state 3 is given by

$$p_3 = S_{x_3} - \sigma_3 = -151.9038e^6 - -353.1726e^6 = 201.2688 \text{ MPa}$$

With the deviatoric stresses known, the hypothesis that the solution is elastic can be tested by applying the yield criterion Eq.[2.58]

$$\frac{3}{2}|S_x| = \frac{3}{2}|-151.9038| = 227.8 \text{ MPa} \leq \bar{\sigma} = 300 \text{ MPa}$$

Since the effective stress is below the yield surface, the hypothesis that the response was elastic is correct. All other properties at states 2 and 3 will be identical to the hydrostatic case.

### Elastic Solution using the Mie-Grueneisen Equation of State

This second method of calculating the elastic response utilizes the Mie-Grueneisen Equation of State which is dependent on the energy equation. The problem definition is the same as in the previous section where twelve unknowns must be matched with twelve independent equations. If the Mie-Grueneisen Equation of State is added to the twelve equations, one other equation must be removed such that the total number remain at twelve. The only possible solution is to replace the Experimental Hugoniot with the Mie-Grueneisen Equation of State.

It is tempting to conclude that since the Mie-Grueneisen Equation of State derived in Section [2.1.5] uses the the Experimental Hugoniot in its derivation, that the Experimental Hugoniot must still be available for the calculation of the shock speeds as in the previous example. This assumption is false. It is true that the Mie-Grueneisen Equation of State as implemented calculates reference Hugoniot values using the Experimental Hugoniot. However, that assumption is only valid within the context of the derivation of the reference Hugoniot and may not necessarily be available outside that context.

The Mie-Grueneisen Equation of State has a very complex dependency on density as observed in Eq.[2.121]. This complexity makes it difficult to form explicit closed form solutions for all but very simple problems, thus numerical techniques are needed to algebraically solve for the unknown states.

To calculate the jump conditions across a discontinuity as in Fig. [2.1], consider that  $\rho_2$  and all parameters at state 1 are known. From the Hugoniot Equation given by Eq.[2.36], the jump in energy is implicitly solved giving



$$e_2 = \frac{e_1 + \frac{1}{2} \left( \sigma_1 + S_x(\rho_2) - P_H(V_2) \left[ 1 - \frac{\Gamma}{2V_2} (V_0 - V_2) \right] \right) (V_2 - V_1)}{1 + \frac{\Gamma}{2V_2} (V_2 - V_1)} \quad (2.68)$$

where  $S_x(\rho_2)$  is given by Eq.[2.64] and  $P_H(\rho_2)$  is given by Eq.[2.120]. The normal stress is given by

$$\sigma_2 = S_x(\rho_2) - P(e_2, V_2) \quad (2.69)$$

with the velocity jump solved using Eq.[2.37] resulting in

$$v_2 = v_1 - \sqrt{(\sigma_2 - \sigma_1)(V_2 - V_1)} \quad (2.70)$$

where the negative root corresponds to a left-running wave. For a right running wave

$$v_2 = v_1 + \sqrt{(\sigma_2 - \sigma_1)(V_2 - V_1)} \quad (2.71)$$

where the positive root corresponds to a right-running wave.

The difficulty using the previous analysis is that specification of density at state 2 is inconvenient for solving the shock impact problem. Ideally, velocity at state 2 is determined by satisfying continuity in normal stress at the contact discontinuity, then using the velocity to solve for the remaining conditions at state 2 and 3.

To accomplish this, a numerical procedure is defined with an error function defined as

$$f(\rho_2) = v(\rho_2) - U_c \quad (2.72)$$

where  $v(\rho_2)$  is the procedure which produces velocity in Eq.[2.70] given density  $\rho_2$  and the desired contact discontinuity velocity  $U_c$ . To generate a new density which reduces the error in Eq.[2.72] from some initial estimate of density  $\rho_i$ , the following function

$$\rho_{i+1} = \rho_i - \frac{f(\rho_i)}{f'(\rho_i)} \simeq \rho_i - \Delta\rho \left( \frac{v(\rho_i) - U_c}{u(\rho_i + \Delta\rho) - v(\rho_i)} \right) \quad (2.73)$$

is iterated until  $|\rho_{i+1} - \rho_i| < \epsilon$ . The method is functionally a Newton-Raphson technique where the derivatives are evaluated using a first order finite difference approximation. The parameters  $\epsilon$  and  $\Delta\rho$  are reasonably small values taken during this study to be  $1.0e^{-12}$  and 0.01, respectively. Convergence usually requires two or three iterations and is very robust.

To calculate the contact discontinuity speed  $U_c$ , Eq.[2.52] is used if the material and thermodynamic properties are identical. If this is not the case, then the result of the previous numerical procedure will not produce a correct normal stress at the contact discontinuity, i. e.  $\sigma_2 \neq \sigma_3$ . To correct this problem, a second numerical procedure is constructed to iterate the contact discontinuity speed to convergence. Eq.[2.52] is used to approximate  $U_c$  and an error function is constructed assuming that the normal stress is a function of velocity where

$$f(v_2, v_3) = \sigma_3(v_3) - \sigma_2(v_2) \quad (2.74)$$

With this function a similar numerical procedure is established with the outside loop calculating the contact discontinuity speed and the inside loops calculating state properties based on that velocity. However, this choice of error functions is not tolerant of parameters that stray far from the symmetry conditions. An alternative error function might enforce the Hugoniot Equation Eq.[2.36] at the contact discontinuity such that

$$f(\rho_2, \rho_3) = e_2(\rho_2) - e_3(\rho_3) - \frac{1}{2}(\sigma_2 + \sigma_3)\left(\frac{1}{\rho_3} - \frac{1}{\rho_2}\right) \quad (2.75)$$

though this function has not been investigated thoroughly to report on. The shock speed for the reflected shock is calculated by solving Eq.[2.29] for  $U_{rs}$  resulting in

$$U_{rs} = \frac{\rho_1 v_1 - \rho_2 v_2}{\rho_1 - \rho_2} \quad (2.76)$$

Similarly the shock speed for the transmitted shock is given by

$$U_{ts} = \frac{\rho_3 v_3 - \rho_4 v_4}{\rho_3 - \rho_4} \quad (2.77)$$

**EXAMPLE: Elastic response using the Mie-Grueneisen Equation of State.**

Consider the impact problem as defined in the previous example. The contact discontinuity velocity  $U_c = 0$  m/s will be the same since the configuration is symmetric. The results of the numerical procedure as outlined in the preceding text for an elastic response is shown in Table [2.2]. The shock speed for the reflected shock is calculated using Eq.[2.76] resulting in

$$U_{rs} = \frac{8930.0 \cdot 10.0 - 8948.925 \cdot 0}{8930.0 - 8948.925} = -4718.63 \text{ m/s}$$

Similarly the shock speed for the transmitted shock is given by Eq.[2.77] resulting in

$$U_{ts} = \frac{8948.925 \cdot 0 - 8930.0 \cdot (-10.0)}{8948.925 - 8930.0} = 4718.63 \text{ m/s}$$

Note that the value of internal energy using the Mie-Gruneisen equation of state matches that for the elastic solution given by the Experimental Hugoniot even though the pressure and density vary between the two solutions. This result is somewhat unexpected due to the complexity of the expression for energy given by Eq.[2.68] as compared to the expression using the Experimental Hugoniot given by Eq.[2.36]. This suggests that a simpler approach might be available for the solution using the Mie-Gruneisen equation of state, though the explanation of this phenomena remains a mystery. This point certainly needs further investigation.

The results for state 3 are the same as for state 2 as shown in Table [2.2].

Table 2.2: Results of the numerical procedure for the shock impact problem for state 2 using the Mie-Grueneisen Equation of State.

$v_2$	$= 0 \text{ m/s}$
$\rho_2$	$= 8948.93 \text{ Kg/m}^3$
$p_2$	$= 295.29 \text{ Mpa}$
$e_2$	$= 50.0 \text{ J/Kg}$
$S_{x_2}$	$= -126.98 \text{ Mpa}$
$\sigma_{x_2}$	$= -422.27 \text{ Mpa}$

### Two-wave response using the Experimental Hugoniot

When the effective stress exceeds the elastic limit on the yield surface, the material response becomes plastic and is accompanied by a change of slope on the stress-strain curve as shown in Figure [2.5]. When this occurs, two shocks may form depending on the requirements for the shock speeds. The fastest wave is called the elastic pre-cursor and compresses the material to the elastic limit. The second shock, if it exists, is referred to as the “plastic shock” as its existence is due to the plastic response of the material.

For this case the impact of the two bars results in six states as illustrated in Figure.[2.4]. Though it is possible for one material to have an elastic response and the other a plastic response, those cases will not be considered, though the treatment is straightforward. The deviatoric stress generated behind the elastic pre-cursor at states 1' and 4' reaches a maximum defined by the yield surface or

$$-\frac{2}{3}\bar{\sigma}^Y = S_{x_{1'}} = S_{x_{4'}} \quad (2.78)$$

where the negative sign assumes compression. Since the deviatoric stress is known at states 1', the density can be calculated from Eqs.[2.64] where

$$\rho_{1'} = \rho_1 \exp \left[ \frac{3}{4GL} (S_{x_1} - S_{x_{1'}}) \right] \quad (2.79)$$

Similarly for state 4'

$$\rho_{4'} = \rho_4 \exp \left[ \frac{3}{4GR} (S_{x_4} - S_{x_{4'}}) \right] \quad (2.80)$$

The velocity at state 1' can be calculated by combining the expression for the left-moving Experimental Hugoniot Eq.[2.40] and mass continuity Eq.[2.42] to provide

$$v_{1'} = v_1 + \frac{c_0^L(\rho_{1'} - \rho_1)}{s^L(\rho_{1'} - \rho_1) - \rho_{1'}} \quad (2.81)$$

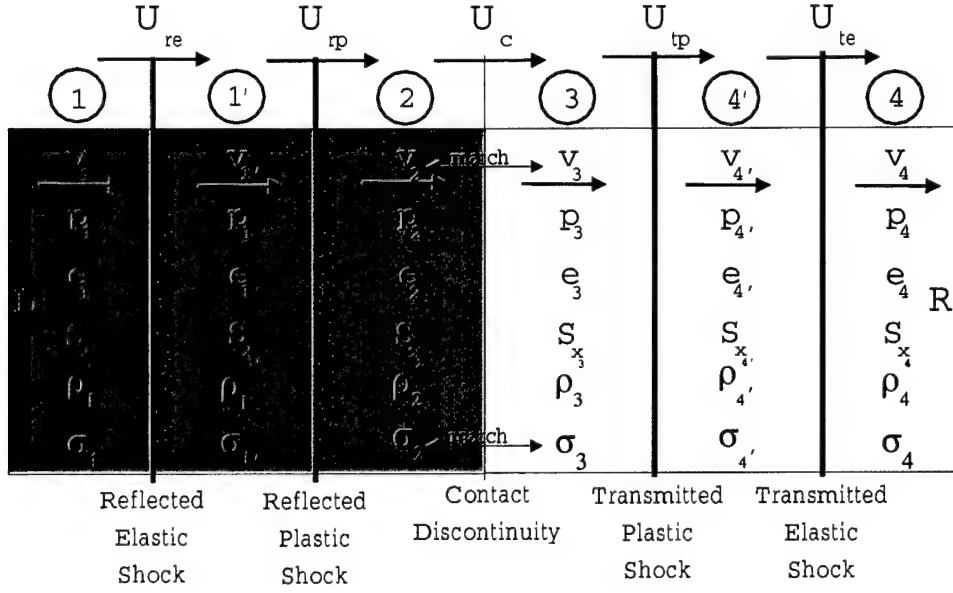


Figure 2.4: Figure illustrating the two-wave Plastic Solution.

Similarly for state 4'

$$v_{4'} = v_4 + \frac{-c_0^R(\rho_{4'} - \rho_4)}{s^R(\rho_{4'} - \rho_4) - \rho_{4'}} \quad (2.82)$$

The shock speed  $U_{re}$  is calculated from Eqs.[2.40] to give

$$U_{re} = v_1 - c_o^L + s^L(v_{1'} - v_1) \quad (2.83)$$

Similarly, the shock speed  $U_{te}$  is calculated from Eq.[2.39] to give

$$U_{te} = v_4 + c_0^R + s^R(v_{4'} - v_4) \quad (2.84)$$

The normal stress can be computed from Eq.[2.44] at state 1' using

$$\sigma_{1'} = \sigma_1 + \rho_1(U_{re} - v_1)(v_1 - v_{1'}) \quad (2.85)$$

and similarly at state 4' as

$$\sigma_{4'} = \sigma_4 + \rho_4(U_{te} - v_4)(v_4 - v_{4'}) \quad (2.86)$$

Pressure at state 1' is calculated by

$$p_{1'} = S_{x_{1'}} - \sigma_{1'} \quad (2.87)$$

and similarly for state 4'

$$p_{4'} = S_{x_{4'}} - \sigma_{4'} \quad (2.88)$$

Energy can be computed using the Hugoniot Equation [2.36] resulting in

$$e_{1'} = e_1 + \frac{1}{2}(\sigma_1 + \sigma_{1'})(V_{1'} - V_1) \quad (2.89)$$

and similarly for state 4' where

$$e_{4'} = e_4 + \frac{1}{2}(\sigma_4 + \sigma_{4'})(V_{4'} - V_4) \quad (2.90)$$

Note that the solution for state 1' and 4' does not depend on the velocity of the contact discontinuity as in previous examples. The states at 1' and 4' are completely determined by the elastic yield stress. However, this is not the case for states 2 and 3.

If the material response is purely plastic, i. e.  $H' = 0$ , then a shock is necessary because of a thermodynamic mismatch between states 1' and 2, and similarly, between states 4' and 3. The deviatoric stress across the plastic shock will be continuous since the bar cannot unload and the yield surface constrains the deviatoric stress from increasing. Given the speed of the contact discontinuity  $U_c$ , the shock speeds  $U_{rp}$  and  $U_{lp}$  can be determined from the Experimental Hugoniot relation, and the rest of the unknowns at states 2 and 3 follow the same procedure as for a hydrostatic shock (See Section [2.1.2]) where states 1 and 4 in the hydrostatic solution are replaced with 1' and 4', respectively.

For a material with  $H' > 0$ , then in addition to the thermodynamic jump described in the previous paragraph, there would be an additional production of deviatoric stress from plastic compression governed by Eq.[2.19d]. The yield surface itself depends on the production of plastic strain  $\bar{\epsilon}$  governed by Eq.[2.19e]. These two production equations can be combined to relate stress and plastic strain similar to the elastic case. The ratio of Eq.[2.19d] and Eq.[2.19e] gives

$$\frac{\frac{dS_x}{dt}}{\frac{d\bar{\epsilon}}{dt}} = \frac{\frac{4}{3}G(1-\beta)v_x}{\frac{2}{3}f\beta v_x} = 2G\left(\frac{1}{\beta} - 1\right)f = \frac{dS_x}{d\bar{\epsilon}} \quad (2.91)$$

where  $f = \text{Sign}(v_x)$ . In a compressive environment,  $v_x < 0$ , therefore,  $f = -1$ . Rewriting Eq.[2.91] in a differential form leaves

$$dS_x = 2G\left(1 - \frac{1}{\beta}\right)d\bar{\epsilon} \quad (2.92)$$

For elastic strain,  $d\epsilon = \frac{dl}{l}$ , but the current definition of elastic strain requires that  $\bar{\epsilon} > 0$  which is violated in compression. To compensate for this, plastic strain will be defined in terms of  $\bar{l}$  where

$$d\bar{\epsilon} \equiv -\frac{d\bar{l}}{\bar{l}} \quad (2.93)$$

Substituting Eq.[2.93] into Eq.[2.92] leaves

$$dS_x = 2G\left(\frac{1}{\beta} - 1\right) \frac{d\bar{l}}{\bar{l}} \quad (2.94)$$

Integrating Eq.[2.94] from the elastic yield point  $S_x^Y$  to the resting point on the yield surface provides

$$\int_{S_x^Y}^{S_x} dS_x = 2G\left(\frac{1}{\beta} - 1\right) \int_{\bar{l}_0}^{\bar{l}} \frac{d\bar{l}}{\bar{l}}$$

or,

$$\begin{aligned} S_x - S_x^Y &= 2G\left(\frac{1}{\beta} - 1\right) \left[ \ln \bar{l} \right]_{\bar{l}_0}^{\bar{l}} \\ S_x - S_x^Y &= 2G\left(\frac{1}{\beta} - 1\right) (\ln \bar{l} - \ln \bar{l}_0) = 2G\left(\frac{1}{\beta} - 1\right) \ln \frac{\bar{l}}{\bar{l}_0} \end{aligned} \quad (2.95)$$

As in the elastic case for uniaxial strain, volumetric and longitudinal strain are identical, therefore

$$\frac{\bar{l}}{\bar{l}_0} = \frac{V}{V_0} = \frac{\rho_0}{\rho} \quad (2.96)$$

Substituting the equation above in Eq.[2.95] results in

$$S_x = S_{x_0}^Y + 2G\left(\frac{1}{\beta} - 1\right) \ln \frac{\rho_0}{\rho} \quad (2.97)$$

Rewriting this equation in the context of state 2 from Fig.[2.4]

$$S_{x_2} = S_x^Y|_L + 2G\left(\frac{1}{\beta^L} - 1\right) \ln \frac{\rho_{1'}}{\rho_2} \quad (2.98)$$

and for state 3 the equivalent expression is

$$S_{x_3} = S_x^Y|_R + 2G\left(\frac{1}{\beta^R} - 1\right) \ln \frac{\rho_{4'}}{\rho_3} \quad (2.99)$$

However, at this point  $S_{x_2}$  and  $S_{x_3}$  can not be calculated because the densities at those states are unknown. However, the speed of the contact discontinuity  $U_c = v_2 = v_3$  can be calculated as in the solution of Eq.[2.46] where state 1 is replace with 1' and state 4 with 4'. The shock speeds  $U_{rp}$  and  $U_{tp}$  follow suit from Eq.[2.40] and Eq.[2.39], respectively, where

$$U_{rp} = v_{1'} - c_0^L + s^L(v_2 - v_{1'}) \quad (2.100)$$

and

$$U_{tp} = v_{4'} - c_0^R + s^R(v_3 - v_{4'}) \quad (2.101)$$

The densities at states 2 and 3 can be calculated from Eq.[2.42] and Eq.[2.43] as

$$\rho_2 = \rho_{1'} \frac{U_{rp} - v_{1'}}{U_{rp} - v_2} \quad (2.102)$$

and

$$\rho_3 = \rho_{4'} \frac{U_{tp} - v_{4'}}{U_{tp} - v_3} \quad (2.103)$$

Now that the densities are known at states 2 and 3, the deviatoric stresses in Eq.[2.98] and Eq.[2.99] can be calculated.

The normal stresses at states 2 and 3 are calculated from Eq.[2.44] and Eq.[2.45] as

$$\sigma_2 = \sigma_{1'} + \rho_{1'}(U_{rp} - v_{1'})(v_{1'} - v_2) \quad (2.104)$$

and

$$\sigma_3 = \sigma_{4'} + \rho_{4'}(U_{tp} - v_{4'})(v_{4'} - v_3) \quad (2.105)$$

Pressures are calculated directly as

$$p_2 = S_{x_2} - \sigma_2$$

and

$$p_3 = S_{x_3} - \sigma_3$$

and energies are calculated from Eq.[2.55] and Eq.[2.56] as

$$e_2 = e_{1'} + \frac{1}{2}(p_{1'} + p_2)(V_{1'} - V_2) \quad (2.106)$$

and

$$e_3 = e_{4'} + \frac{1}{2}(p_{4'} + p_3)(V_{4'} - V_3) \quad (2.107)$$

An example for this case will not be given because while it has academic value, a two wave system given the current material properties is not possible without an unrealistically high yield stress, therefore the example will be left to the interested reader.

### 2.1.3 Two-wave response using the Mie-Grueneisen Equation of State.

The description for the two-wave response is very similar to the case for the Experimental Hugoniot, except of course that the Experimental Hugoniot is being replaced with the Mie-Grueneisen Equation of state. The deviatoric stress and density at state 1' and 4' will be identical. Once the density is known, the Hugoniot curve Eq.[2.36] is expanded in terms of the deviatoric stress and pressure at state 1'. Solving implicitly (See Eq.[2.115]) for energy at state 1' leaves the rather lengthy expression

$$e_{1'} = \frac{e_1 + \frac{1}{2} \left( \sigma_1 + S_x(\rho_{1'}) - p_H(V_{1'}) \left[ 1 - \frac{\Gamma}{2V_{1'}}(V_0 - V_{1'}) \right] \right) (V_{1'} - V_1)}{1 + \frac{\Gamma}{2V_{1'}}(V_{1'} - V_1)} \quad (2.108)$$

The pressure at state 1' is found by solving the Hugoniot Equation Eq.[2.36] for pressure or

$$p_{1'} = S_{x_{1'}} + \sigma_1 - \frac{2 \cdot (e_{1'} - e_1)}{V_{1'} - V_1} \quad (2.109)$$

The velocity is found from Eq.[2.70] as

$$v_{1'} = v_1 - \sqrt{(\sigma_{1'} - \sigma_1)(V_{1'} - V_1)} \quad (2.110)$$

where  $\sigma_{1'} = S_{x_{1'}} - p_{1'}$ . The velocity for state  $v_{4'}$  is found from Eq.[2.71] as

$$v_{4'} = v_4 + \sqrt{(\sigma_{4'} - \sigma_4)(V_{4'} - V_4)} \quad (2.111)$$

thereby completing the unknowns at state 1'.

The states at 2 and 3 must be determined numerically as was the case with the elastic solution using the Mie-Grueneisen Equation of State. The contact discontinuity speed is calculated or approximated using

$$v_c = \frac{1}{2}(v_1 + v_4) \quad (2.112)$$



The numerical procedure developed in Section 2.1.2 is used where  $S_x(\rho_2)$  uses the plastic function as defined in Eq.[2.98]. The states at 2 and 3 are calculated, then if the normal stresses are not equal at the contact discontinuity, the densities at states 2 and 3 are recalculated using a Newton-Raphson procedure as developed earlier until the error tolerance is below the established criteria.

**EXAMPLE: Two-wave solution using the Mie-Grueneisen Equation of State.**

The physical orientation will be the same as in previous examples and the material values will be the same as in Table 2.1. The initial properties at states 1 and 4 will be the same as in the previous examples except that  $v_1 = 100 \text{ m/s}$ . The problem is to find the states at 1', 2, 3, and 4'.

The problem is the collision of two like metal bars which impact on another. The physical properties are given in Table 2.1 except that  $H_b$  will be set to zero such that the response is purely plastic. The initial conditions in the bars will be  $p_1 = p_4 = 0.0$ ,  $e_1 = e_4 = 0.0$ ,  $S_{x_1} = S_{x_4} = 0.0$ . The velocity of the left bar will be  $v_1 = 100 \text{ m/s}$  and the velocity of the right bar will be  $v_4 = -100 \text{ m/s}$ .

The assumption is made that the deviatoric stress exceeded the yield point assuming an elastic response, thus the solution must exhibit a plastic response. However, to have a two-wave system the shock speed of the plastic wave must be less than the shock speed of the elastic wave. If this is not the condition, then the shocks will coalesce into a single shock. From Eq.[2.78] we have that  $S_{x_{1'}} = S_{x_{4'}} = \frac{2}{3} \cdot 300 = -200 \text{ Mpa}$  in compression. From Eq.[2.79], we can calculate the density at state 1' as

$$\rho_{1'} = 8930.0 \cdot \exp \left[ \frac{3.0}{4.0 \cdot 45.0e^9} (0.0 - (-200.0 \cdot 10^6)) \right] = 8959.816332 \text{ Kg/m}^3$$

The calculation of energy at state 1' will be broken into several pieces to simplify the solution. The reference Hugoniot  $p_H(\rho_{1'})$  is given by Eq.[2.120] or

$$p_H(\rho_{1'}) = \frac{3940.0^2 \cdot \left( \frac{1}{8930.0} - \frac{1}{8959.816332} \right)}{\left[ 1.49 \cdot \left( \frac{1}{8930.0} - \frac{1}{8959.816332} \right) - \frac{1}{8930.0} \right]^2} = 466.077 \text{ MPa}$$

The energy is solved using Eq.[2.108]

$$e_{1'} = \frac{0.0 + \frac{1}{2} \left( 0.0 + -200 \cdot 10^6 - 466.077 \cdot 10^6 \left[ 1 - \frac{2.0}{2 \cdot \frac{1}{8959.816332}} \left( \frac{1}{8930} - \frac{1}{8959.816332} \right) \right] \right) \left( \frac{1}{8959.816332} - \frac{1}{8930} \right)}{1 + \frac{2.0}{2 \cdot \frac{1}{8959.816332}} \left( \frac{1}{8959.816332} - \frac{1}{8930} \right)}$$

$$e_{1'} = 124.272 \text{ J/Kg}$$

The pressure is found at state 1' using Eq.[2.109] where

$$p_{1'} = -200.0 \cdot 10^6 + 0.0 - \frac{2 \cdot (124.272 - 0.0)}{\frac{1}{8959.816332} - \frac{1}{8930.0}} = 466.744826 \text{ MPa}$$

The normal stress at state 1' is

$$\sigma_{1'} = S_{x_{1'}} - p_{1'} = -200 \cdot 10^6 - 466.744826 \cdot 10^6 = -666.744 \text{ MPa}$$

The velocity is found at state 1' using Eq.[2.70]

$$v_{1'} = 100.0 - \sqrt{\left(-666.744e^6 - 0.0\right) \left(\frac{1}{8959.826} - \frac{1}{8930.0}\right)} = 84.23 \text{ m/s}$$

The shock speed  $U_{re}$  is calculated using Eq.[2.29] where

$$U_{re} = \frac{8930.0 \cdot 100.0 - 8959.826 \cdot 84.2347}{8930.0 - 8959.826} = -4635.95 \text{ m/s}$$

The properties at state 4' are identical to state 1' except the velocity which is calculated from Eq.[2.71] which is

$$v_{4'} = -100.0 + \sqrt{\left(-666.744e^6 - 0.0\right) \left(\frac{1}{8959.826} - \frac{1}{8930.0}\right)} = -84.23 \text{ m/s}$$

The shock speed  $U_{rp}$  is calculated from Eq.[2.29] where

$$U_{rp} = \frac{8959.826 \cdot 84.2347 - 9147.919 \cdot 0}{8959.826 - 9147.919} = -4012.535 \text{ m/s}$$

Summarizing the solution at state 1':

$$\begin{aligned}\rho &= 8959.816332 \text{ Kg/m}^3 \\ v &= 84.23 \text{ m/s} \\ p &= 466.744826 \text{ MPa} \\ S_x &= -200 \text{ MPa} \\ \sigma &= -666.744 \text{ Mpa} \\ e &= 124.272 \text{ J/Kg}\end{aligned}$$

and summarizing the results at state 4'

$$\begin{aligned}\rho &= 8959.816332 \text{ Kg/m}^3 \\ v &= -84.23 \text{ m/s} \\ p &= 466.744826 \text{ MPa} \\ S_x &= -200 \text{ MPa} \\ \sigma &= -666.744 \text{ Mpa} \\ e &= 124.272 \text{ J/Kg}\end{aligned}$$

The conditions at state 2 and 3 are solved using the described numerical procedure with the results presented in Table 2.1.3.

Table 2.3: Result of numerical procedure at states 2 and 3 using the Mie-Grueneisen equation of state for the two wave problem.

---

$\rho$	$= 9147.919 \text{ Kg/m}^3$
$v$	$= 0 \text{ m/s}$
$p$	$= 3.559 \text{ GPa}$
$S_x$	$= -200.0 \text{ MPa}$
$\sigma$	$= -3.7587 \text{ GPa}$
$e$	$= 5219.884 \text{ J/Kg}$

---

#### 2.1.4 Single-wave plastic response using the Mie-Grueneisen Equation of State.

If the contact discontinuity velocity increases in a two-wave system, at some point the velocity of the plastic wave will equal the velocity of the elastic wave. When this happens, the shocks collapse back to a single wave system as shown in Fig.[2.2]. The production of deviatoric stress at state 2 is taken from Eq.[2.98] where

$$S_{x_2} = S_x^Y|_L + 2G\left(\frac{1}{\beta^L} - 1\right) \ln \frac{\rho_1}{\rho_2} \quad (2.113)$$

and similarly for state 3

$$S_{x_3} = S_x^Y|_R + 2G\left(\frac{1}{\beta^R} - 1\right) \ln \frac{\rho_4}{\rho_3} \quad (2.114)$$

The numerical procedure used in Section 2.1.2 is used to generate the parameters at state 2 and 3.

#### EXAMPLE: Single Wave Plastic Solution using the Mie-Grueneisen Equation of State.

For this case the velocity at state 1 will be increased to  $v_1 = 600 \text{ m/s}$  with  $v_4 = -600.0 \text{ m/s}$ . The numerical procedure as described previously will be employed to solve for the unknown states at 2 and 3. The results of this procedure are shown in Table 2.4.

#### 2.1.5 The Equation of State

A convenient and often used equation of state for shock related problems is the Mie-Grueneisen equation of state, which gives pressure in terms of internal energy and specific volume or density as follows:

$$p(e, V) = p_H(V) + \frac{\Gamma}{V}(e - e_H(V)) \quad (2.115)$$

Its convenience in part stems from the use of the shock Hugoniot to give reference values. The pressure at an arbitrary value of specific volume and internal energy  $p(e, V)$  is obtained by finding the pressure  $p_H(V)$

Table 2.4: Result of numerical procedure for states 2 and 3 using the Mie-Grueneisen equation of state for the single plastic wave problem.

---

$\rho$	$=$	$10189.95 \text{ Kg/m}^3$
$v$	$=$	$0.0 \text{ m/s}$
$p$	$=$	$25.8 \text{ GPa}$
$e$	$=$	$.18045 \text{ MJ/Kg}$
$S_x$	$=$	$-200.0 \text{ MPa}$
$\sigma$	$=$	$-26.0 \text{ GPa}$

---

and internal energy  $e_H(V)$  on a reference Hugoniot at a given density. The variation of the desired energy from the Hugoniot energy is then linearly related to the pressure difference at the fixed density, with the proportionality constant being  $\frac{\Gamma}{V}$ , where  $\Gamma$  is the Grueneisen coefficient.

The Hugoniot reference state with a specified density  $\rho_H$  must satisfy the Rankine-Hugoniot relations with a “zero state” where pressure, energy, and velocity are zero, i. e.  $p_0 = e_0 = v_0 = 0$ , with specified density  $\rho_0$ . Letting 1 state in Eq.[2.35] be the “zero state” and state 2 be the Hugoniot reference state, then

$$e_H(V_H) = \frac{p_H}{2}(V_0 - V_H) \quad (2.116)$$

Using the same substitution in Eq.[2.37] and solved for  $p_H$  leaves

$$p_H(V_H) = \frac{v_H^2}{V_0 - V_H} \quad (2.117)$$

If the above equation is substituted in Eq.[2.116], then

$$e_H = \frac{v_H^2}{2} \quad (2.118)$$

Substituting Eq.[2.118] into Eq.[2.115] results in

$$p(e, V) = p_H(V) \left[ 1 - \frac{\Gamma}{2V}(V_0 - V) \right] + \frac{\Gamma}{V}e \quad (2.119)$$

The reference Hugoniot state including the shock speed has 4 unknowns, i. e. the speed of the discontinuity  $U_s$ ,  $v_H$ ,  $e_H$ , and  $p_H$ . There are only three Rankine-Hugoniot equations, thus some other equation must be supplied to complete the system of unknowns at the reference Hugoniot<sup>2</sup>. The Experimental Hugoniot will be used for this purpose. Combining Eq.[2.37] and either of Eqs.[2.39] or Eq.[2.40] results in

<sup>2</sup>If the Mie-Grueneisen were designed such that the reference pressure were a function of energy as well as specific volume, then Eq.[2.116]-Eq.[2.118] would be sufficient to define the reference Hugoniot state.

$$p_H(V) = \frac{c_0^2(V_0 - V)}{[s(V_0 - V) - V_0]^2} \quad (2.120)$$

Substituting this expression into Eq.[2.119] leaves

$$p(e, V) = \frac{c_0^2(V_0 - V)}{[s(V_0 - V) - V_0]^2} \left[ 1 - \frac{\Gamma}{2V}(V_0 - V) \right] + \frac{\Gamma}{V}e \quad (2.121)$$

which is the Mie-Grueneisen Equation of State. This empirical condition, where  $s$  and  $c_0$  are material constants, is particularly useful both because of its simplicity and that it has been experimentally verified to represent many materials quite well.

## 2.2 Numerical Aspects

This section presents the numerical algorithms used to simulate the impact dynamics of uniaxial strain. Subsection 2.2.1 presents the methods used to integrate the mass continuity, momentum, and energy equations cast in an Eulerian reference frame using a strictly conservative integration method. Section 2.2.2 describes upwind approaches for evaluating the flux used in the integration of the conservative equations in a manner which is essentially non-oscillatory without the need for explicit dissipative dampening. Section 2.2.3 derives the eigenvalues required to construct the characteristic velocity used in the integration scheme. The last section 2.2.5 describes the technique developed to avoid applying the traditional "Turning Method" when the numerical algorithm transitions from the elastic to the plastic portion of the surface.

### 2.2.1 Integration Scheme for the Conservation Equations

The equations of motion as presented from an Eulerian perspective, do not implicitly solve for the deformation of the continuum, but rather solve for the unknown velocity field. In contrast, Lagrangian techniques assume a material perspective and therefore track the material motion as the deformation occurs. The disadvantage of the latter is that the discretization of the deformed media can become highly skewed resulting in reduced accuracy. On the other hand, the Eulerian technique allows mass to pass through the internal cell structures providing the opportunity for the numerical technique to adjust the nodal placement within the continuum. The current philosophy is to require that nodes which lie on material boundaries remain on the boundaries for all time, whereas the interior nodes may deform in any manner to maintain the accurate solution of the problem. The requirement that boundary nodes remain on the boundary enters the solution as a boundary condition where

$$\frac{\partial x_i}{\partial t} = g(v_i) \text{ for } x_i \in [\text{boundary}] \quad (2.122)$$

Note that  $g(v_i)$  for the multidimensional case does not require the boundary nodes to move at local particle velocities (though this would be a solution), but simply requires that the boundary nodes lie on the surface of the deformed material. This condition is also used to specify collisions with other surfaces, or a free boundary which evolves with the solution. Grid motion on the interior given by

$$\frac{\partial x_i}{\partial t} = h(v_i) \text{ for } x_i \in [\textit{interior}] \quad (2.123)$$

can support any function  $h(v_i)$  which is compatible with the boundary deformation to achieve a desirable nodal distribution. However the grid advection speed contributes to the eigenvalues of the system and since the maximum time step is inversely proportional to the maximum eigenvalue of the system, functions which move the interior nodes against the particle motion can significantly reduce the time step taken by the integration algorithm. For this reason, care should be taken when choosing  $h(v_i)$  to minimize this influence.

While the Eulerian form of the equations of motion provides additional flexibility in the discretation of the domain, this flexibility adds complexity to the integration of the equations of motion. To illustrate this, consider the divergence form of the one-dimensional equations of motion given by

$$\frac{\partial U}{\partial t} + \frac{\partial f}{\partial x} = 0 \quad (2.124)$$

The equation is integrated over an arbitrary control volume resulting in

$$\oint_V \frac{\partial U}{\partial t} dV + \oint_V \frac{\partial f}{\partial x} dV = 0 \quad (2.125)$$

Gauss's Theorem is used to represent the second term as a surface integral giving

$$\oint_V \frac{\partial U}{\partial t} dV + \oint_S (f \cdot \hat{n}) dS = 0 \quad (2.126)$$

Here, the surface  $S$  bounds the control volume  $V$ , and  $\hat{n}$  is a unit outward normal on the surface  $S$ . The volume and the control surface are assumed to be constant during integration, therefore Eq.[2.126] can not be used to integrate the equations of motion if the grid is deforming. This concept and the issues surrounding a moving grid for Eulerian equations lead to the definition of the so-called Geometric Conservation Law[7] or GCL. A recent investigation conducted by [8] determined that if the numerical solution could exactly reproduce a constant flow field subjected to grid motion, then the solution was at least first-order accurate in time. However, no options were offered for schemes requiring a higher level of temporal accuracy. Is it therefore possible to have a method which is at least second-order accurate in time with a moving mesh? Fortunately, the answer is that *any order* of temporal accuracy is possible if the integration of the equations of motion properly account for the deformation of the grid.

The fundamental problem of integrating Eq.[2.126] subjected to a moving mesh comes as the result of the conventional wisdom of separating the time derivative from the spatial derivatives before the application of Gauss' Theorem. As early as 1968, [9] and later [10] recognized that the divergence form of the equations of motion could include time as a coordinate direction, thus the nabla or del operator  $\nabla$  could be written in the three-dimensional form for cartesian components as

$$\nabla \equiv \left( \frac{\partial}{\partial t} \hat{e}_t + \frac{\partial}{\partial x} \hat{e}_x + \frac{\partial}{\partial y} \hat{e}_y + \frac{\partial}{\partial z} \hat{e}_z \right) \quad (2.127)$$

For the one-dimensional problem, the volume represents an  $(t,x)$  area. For a two-dimensional problem the volume is a  $(t,x,y)$  time-space slab, and a three-dimensional problem produces a  $(t,x,y,z)$  four-dimensional volume. With this operator, the conservation equations can now be represented in the simple divergence form as

$$\nabla \cdot F = S(U) \quad (2.128)$$

where  $F = (U, \mathbf{f})$ . The volume integral can now be applied over Eq.[2.128] with deforming geometry without any special consideration as this new definition of volume  $\mathcal{V}$  is constant over the integral giving

$$\oint_{\mathcal{V}} (\nabla \cdot F) d\mathcal{V} = \oint_{\mathcal{V}} S(U) d\mathcal{V} = S_0 \mathcal{V} \quad (2.129)$$

To evaluate the right-hand side of Eq.[2.128], the well known Mean-Value Theorem is applied where  $S_0$  is the value of  $S(U)$  evaluated at some interior point in the volume. In practice, it might be better to use some form of numerical quadrature to produce a more accurate result. The simplification for the current research is better justified in that  $S(U) = 0$  in the absence of body forces which are neglected in this study. For completeness however, the term is left in the derivation.

Applying Gauss's Theorem to the left-hand side, Eq.[2.129] is rewritten for the one-dimensional equation set as

$$\oint_S (F \cdot \hat{\eta}) dS = \oint_S (U \hat{\eta}_t + f \hat{\eta}_x) dS = S_0 \mathcal{V} \quad (2.130)$$

where  $\hat{\eta} = (\hat{\eta}_t, \hat{\eta}_x)$  is a unit outward normal to the control volume. Applying the discrete analogy of Eq.[2.130] to each edge of the control volume leaves

$$\sum_{j=1}^4 (U_j \hat{\eta}_{tj} + f_j \hat{\eta}_{xj}) |S_j| = \sum_{j=1}^4 \mathcal{F}_j = S_0 \mathcal{V} \quad (2.131)$$

Expanding Eq.[2.131] on each surface and solving for the term with  $U_3$  gives

$$(U_3 \Delta x)^{n+1} = (U_1 \Delta x)^n + \mathcal{F}_4^n - \mathcal{F}_2^n + S_0^n V = (U_1 \Delta x)^n + \Delta U_{1,3}^n \quad (2.132)$$

where

$$\Delta U_{1,3}^n = \mathcal{F}_4^n - \mathcal{F}_2^n + S_0^n V \quad (2.133)$$

Eqs.[2.132,2.133] represent a first-order  $\mathcal{O}(\Delta t)$  accurate Euler integration. To extend the method to second-order accuracy, a corrector step is added which is a temporal adaption of the well known MacCormack explicit algorithm [11] which is a member of the Lax-Wendroff method. It's advantage over the classic RK class of schemes is that the predictor step calculates to the  $n+1$  time level, not at some fractional increment.

As a result, boundary conditions applied after the predictor but before the corrector step are straight forward to implement. The two step algorithm is as follows;

$$(U_i \Delta x)^* = (U_i \Delta x)^n + \Delta U_i^n \quad (2.134)$$

$$(U_i \Delta x)^{n+1} = (U_i \Delta x)^* + \frac{1}{2}(\Delta U_i^* - \Delta U_i^n) \quad (2.135)$$

The integration algorithm given above is very efficient requiring only two levels of memory; one level is used to store variables at time level  $n$ , and the second is used to store  $\Delta U$ . The efficiency is gained by storing both levels of  $\Delta U$  in the same array. After  $U^*$  is calculated during the predictor step, the array that holds  $\Delta U^n$  is negated. On the corrector step, the new values of  $\Delta U$  are simply summed into the array holding  $\Delta U^n$ . The corrector step only uses  $U^*$  and  $\Delta U$ 's therefore  $U^*$  calculated during the predictor step can overwrite  $U^n$ . This efficient memory overlap scheme has the added benefit that the same routine that calculates  $\Delta U^n$  will also calculate  $\Delta U^*$ .

The linear stability requirement for this algorithm is

$$\frac{\delta t |c|_{max}}{\Delta x} \leq CFL \leq 1 \quad (2.136)$$

where  $|c|_{max}$  is the maximum eigenvalue of the system, and CFL is the well known Courant-Friedrichs and Lewy number.

## 2.2.2 Flux Evaluation

Most upwind schemes vary only in the method used to compute the interface flux such as  $\mathcal{F}_2$  and  $\mathcal{F}_4$  in Eq.[2.133]. The schemes are designed to damp oscillations in the vicinity of discontinuities while maintaining a sharp profile. For the current application, the dampening of oscillations is particularly critical for the velocity profile where the velocity behind the shock is zero. A small amount of negative velocity will cause the stress to unload thereby creating large perturbations in the stress profile.

Though much work has been done on the development of upwind schemes in the last thirty years (See [12] [13] for an introduction), most of these can be characterized as using one of two fundamental approaches to flux construction; flux interpolation [14][15][22][17], and variable extrapolation followed by flux evaluation[18]. Some of the algorithms having been developed for applications in Computational Fluid Dynamics depend on properties not applicable for the current application. Roe's scheme, for example, depends on the flux function  $F(U)$  being homogeneous of order one in  $U$ , namely,  $AF = U$  which does not hold for the current equation of state[2.121].

Several of the schemes referenced in the previous paragraph were applied with some success to the current application. The CUSP scheme of [15] provided good results if the user was willing to tune the flux limiter for the specific test case. In general, most of the schemes were either too dissipative to prevent the overshoot of shocks, or did not provide enough dissipation resulting in massive oscillations. The scheme providing the best overall performance was the WENO scheme [19] which adaptively computes the best stencil to maximize smoothness of the solution.

Using the notation of [20], we general  $\mathcal{F}_2$  and  $\mathcal{F}_4$  as occurring on a material interface defined by

$$\mathcal{F}_{i+\frac{1}{2}} = \hat{\mathcal{F}}_i^+ + \hat{\mathcal{F}}_{i+1}^- \quad (2.137)$$



where

$$\hat{\mathcal{F}}_i^+ = WENO5(\mathcal{F}_{i-2}^+, \mathcal{F}_{i-1}^+, \mathcal{F}_i^+, \mathcal{F}_{i+1}^+, \mathcal{F}_{i+2}^+) \quad (2.138)$$

$$\hat{\mathcal{F}}_{i+1}^- = WENO5(\mathcal{F}_{i+3}^-, \mathcal{F}_{i+2}^-, \mathcal{F}_{i+1}^-, \mathcal{F}_i^-, \mathcal{F}_{i-1}^-) \quad (2.139)$$

$$\mathcal{F}_i^\pm = \frac{1}{2}(\mathcal{F}(U_i^n) \pm \alpha_i U_i^n) \quad (2.140)$$

and

$$\alpha_i = \text{Max}(|\mathcal{F}'(U_{i-1})|, |\mathcal{F}'(U_i)|, |\mathcal{F}'(U_{i+1})|) \quad (2.141)$$

where  $|\mathcal{F}'(U_i)|$  is the maximum eigenvalue (section 2.2.3). The  $WENO5(a, b, c, d, e)$  operator defines three interpolated values

$$q1 = \frac{a}{3} - \frac{7b}{6} + \frac{11c}{6} \quad (2.142)$$

$$q2 = -\frac{b}{6} + \frac{5c}{6} + \frac{d}{3} \quad (2.143)$$

$$q3 = \frac{c}{3} + \frac{5d}{6} - \frac{e}{6} \quad (2.144)$$

and three smoothness functions

$$IS_1 = 13(a - 2b + c)^2 + 3(a - 4b + 3c)^2 \quad (2.145)$$

$$IS_2 = 13(b - 2c + d)^2 + 3(d - b)^2 \quad (2.146)$$

$$IS_3 = 13(c - 2d + e)^2 + 3(3c - 4d + e)^2 \quad (2.147)$$

The  $WENO5(a, b, c, d, e)$  operator is then defined as

$$WENO5(a, b, c, d, e) = \frac{\omega_1 q1 + \omega_2 q2 + \omega_3 q3}{\omega_1 + \omega_2 + \omega_3} \quad (2.148)$$

where the weights  $\omega_i$  are defined as

$$\omega_i = \frac{1}{(\epsilon + IS_i)^2} \quad (2.149)$$

For all computations,  $\epsilon = 10^{-6}$  as suggested by [20].

The truncation error for the discretation is of order  $\mathcal{O}(\Delta x^5)$  in space and of order  $\mathcal{O}(\Delta t^2)$  in time from Eqs[2.134, 2.135].

### 2.2.3 Eigenvalue Calculation

The Weighted ENO numerical procedure outlined in section 2.2.2 has the advantage that only a single wavespeed is needed (see Eq.[2.141]), unlike other upwind schemes which require the similarity transformation matrices such as the Rieman scheme and others. For a complex equation of state, the calculations can be quite tedious particularly in multiple dimensions.

The wave speed used in Eq.[2.141] is the maximum eigenvalue of the derivative of the flux  $\mathcal{F}(U)$  Eq.[2.130]. The derivative of the flux is given by

$$\frac{\partial \mathcal{F}(U)}{\partial U} = I\eta_t + \frac{\partial f}{\partial U}\eta_x \quad (2.150)$$

or in matrix form as

$$\frac{\partial \mathcal{F}(U)}{\partial U} = \begin{bmatrix} \eta_t & \eta_x & 0 \\ (\frac{\partial p}{\partial \rho} - u^2)\eta_x & \eta_t + u\eta_x(2 - \frac{1}{\rho}\Gamma_0\rho_0) & \frac{1}{\rho}\eta_x\Gamma_0\rho_0 \\ u\eta_x[\frac{(S_x - p)}{\rho} + \frac{\partial p}{\partial \rho} - e_t] & \eta_x\frac{(p - S_x + \rho e_t - u^2\Gamma_0\rho_0)}{\rho} & \eta_t + \eta_x u\frac{\Gamma_0\rho_0}{\rho} \end{bmatrix} \quad (2.151)$$

where

$$\frac{\partial p}{\partial \rho} = \frac{C_0^2\rho_0^2[\Gamma_0(\rho - \rho_0) + s\rho_0 - (1 + s)]}{[\rho(s - 1) - s\rho_0]^3} - \frac{u\Gamma_0\rho_0}{\rho} \quad (2.152)$$

For completeness, the following derivatives were substituted out of Eq.[2.151]

$$\frac{\partial p}{\partial(\rho u)} = \frac{-u\Gamma_0\rho_0}{\rho} \quad (2.153)$$

$$\frac{\partial p}{\partial(\rho e_t)} = \frac{\Gamma_0\rho_0}{\rho} \quad (2.154)$$

The eigenvalues for Eq.[2.151] are

$$\lambda_1 = \eta_t + u\eta_x, \lambda_{(2)} = \lambda_1 \pm c\eta_x \quad (2.155)$$

where  $c$  is defined as

$$c = \sqrt{\frac{\partial p}{\partial \rho} + \frac{[p - Sx + \rho(e_t - u^2)]\Gamma_0\rho_0}{\rho^2}} \quad (2.156)$$

Note that this expression is not equivalent to the sound speed associated with the propagation of acoustic perturbations through the material. To calculate the true sound speed, it is necessary to represent the

stress and strain equations as partial differential equations and include their contributions in the eigenvalue computation.

To complete the definition of  $\alpha_i$  defined in Eq.[2.141], we define

$$|\mathcal{F}(U_i)| \equiv |\lambda_{1i}| + c_i |\eta_{xi}| \quad (2.157)$$

Note that if the grid deforms at the particle velocity rate ( $\frac{dx}{dt} = u$ ), then  $\eta_t = -dx = -u\delta_t$ , and  $\eta_x = \delta_t$  for an outward normal. For this case,  $\lambda_1 = 0$  thus the grid motion was able to eliminate the advective component of the flux leaving only the pressure terms. This reduces the maximum eigenvalue which in turn reduces the amount of dissipation needed for the upwind scheme (Eq.2.140), as well as increasing the overall computational time step. The computational advantage is not dramatic for cases where  $u \ll c$ , but does validate the intuitive notion that the grid should as a general rule move at particle velocity rates when possible.

## 2.2.4 Integration of the Constitutive Equations

The numerical integration technique for the conservation equations provides the mechanism to account for grid deformation both in time and space. To accommodate grid motion for the constitutive equations [2.19d] and [2.19e], a coordinate transformation will be considered where  $t = t(\tau)$ ,  $x = x(\tau, \zeta)$  and inversely  $\tau = \tau(t)$ ,  $\zeta = \zeta(t, x)$ . Applying the chain rule and expanding the transformed equations leaves

$$\frac{dS_x}{d\tau} = (1 - \beta) \frac{4}{3} G \frac{1}{x_\zeta} \frac{\partial u}{\partial \zeta} \quad (2.158)$$

$$\frac{d\bar{\epsilon}}{d\tau} = \beta \frac{2}{3} \frac{1}{x_\zeta} \left| \frac{\partial u}{\partial \zeta} \right| \quad (2.159)$$

where the wave speed  $\zeta_t$  is given by

$$\zeta_t = \frac{u - x_\tau}{x_\zeta} \quad (2.160)$$

Note that the substitution of  $\frac{1}{x_\zeta} \frac{\partial}{\partial \zeta} = \frac{\partial}{\partial x}$  in Eqs.[2.158] and [2.159] reproduces the original equations [2.19d] and [2.19e] except that  $t$  in the original equation is replaced with  $\tau$ . Therefore from the perspective of numerically solving the total differential equations, the transformation may be ignored.

To integrate Eqs.[2.19d,2.19e], assume the equations can be written in the general form

$$\frac{D\phi}{Dt} = f(\phi, t) \quad (2.161)$$

where the partial derivative on the right-hand side has been replaced by some numerical approximation and the function  $f(\phi, t)$  may or may not be an explicit function of  $\phi$  and  $t$ . A second order accurate two-step numerical solution to Eq.[2.161] is given by

$$\phi^* = \phi^n + \delta_t f(\phi^n, t) \quad (2.162)$$

$$\phi^{n+1} = \phi^* + \frac{1}{2} \delta_t \{f(\phi^*, t + \delta_t) - f(\phi^n, t)\} \quad (2.163)$$

Note that the integration procedure is identical to that used for the conservation equations. This is important in that (i) the dependent variables will be at the same point in time after the predictor step thereby simplifying boundary conditions, and (ii) that the schemes share a common linear stability analysis.

### 2.2.5 A Turning Algorithm

The classical numerical procedure for calculating stress and strain rate assumes that the material response during loading is elastic until the effective stress reaches the yield surface. However, the numerical procedure rarely produces a stress exactly on the yield surface and instead generates a forbidden stress above the yield surface. The so-called “Return Methods” treat this problem by geometrically projecting this forbidden stress onto the yield surface using techniques such as the Radial or Oblique Return Method[21]. While these methods have been used with great practical success, their derivation does not strictly satisfy the differential equations for stress and strain rate.

The conventional interpretation of the constitutive equations which govern the stress and strain production is that the transition from elastic to plastic deformation occurs at the yield surface with a slope discontinuity. This mathematical interpretation is commensurate with the concept that the material follows either an elastic or plastic response. While this behavior is approximately correct, a more realistic interpretation is that the transition from elastic to plastic deformation behaves more as a continuous function with a pronounced change of slope at the yield surface. Based on this interpretation, a new method is presented which assumes that the material behavior can be partially plastic at a point *before* the stress violates the yield surface. By selecting the appropriate level of plasticity for the next iteration, the algorithm will compute the value of stress that falls exactly on the yield surface. Since a forbidden stress is never used in the calculation, this method is coined a “Turning Method” as it provides an incremental transition from the elastic to the plastic region<sup>3</sup>.

If the current effective stress is below the yield curve and in loading (point E as shown in Figure.2.5), then an elastic response is assumed and a first order estimate of the stress is calculated. If the resulting effective stress exceeds the yield surface, then the first order estimate is discarded. From this point, the material response is assumed to be in a mixed elastic/plastic mode. To update to the new value of stress and strain, the “Turning Method” utilizes the existing stress and strain rate equations [2.19d] and [2.19e], except that the parameter  $k$  defined in Eq.[2.10] is allowed to take on a fractional value. Casting Eq.[2.19d] and Eq.[2.16] in an incremental form and substituting Eq.[2.10], we have

$$k = \left(1 + \frac{H'}{3G}\right) \left[1 - \frac{1}{2} \frac{f_s \Delta \bar{\sigma}}{G u_x \Delta t}\right] \quad (2.164)$$

where

$$\Delta \bar{\sigma} = H(\bar{\epsilon}_{trial}) - \bar{\sigma}_{elastic} \quad (2.165)$$

---

<sup>3</sup>An early temptation was to refer to this scheme as the “Method of No-Return”. Fortunately, good taste and a more descriptive name won out.

and

$$f_s = \text{Sgn}(S_x) \quad (2.166)$$

where the value  $k$  is assumed constant during this elastic/plastic phase. If  $H'(\bar{\epsilon})$  is zero, then the response is purely plastic and  $\Delta\bar{\sigma}$  is constant resulting in a non-iterative scheme. If  $H'(\bar{\epsilon})$  is non-zero, then  $\bar{\epsilon}_{trial}$  is set to zero in Eq.[2.165],  $\Delta\bar{\sigma}$  is calculated, followed by  $k$  Eq.[2.164], then  $\beta$  Eq.[2.10]. The process is repeated until the change in  $k$  is sufficiently small which in practice requires only a few iterations.

Another way to achieve the same result is to consider that the material is plastic (namely,  $k = 1$ ), but that the slope of the material  $H'$  can be increased beyond what is physical to transition to the yield surface. This equivalent slope can be calculated using  $\beta$  from the current scheme and solving Eq.[2.10] for  $H'$ . This illustrates that the scheme simply clips the edge of the stress-strain curve in order to avoid violating the yield surface.

## 2.3 Numerical Results

To illustrate the accuracy of the numerical algorithm, the test cases presented in the examples will be solved numerically and compared to the exact solutions. The Figures for the examples are shown in Chapter 6.

In order to compute the numerical solution for the hydrostatic and elastic solution using the experimental hugoniot, it was necessary to find a function which expresses pressure as a function of known properties, which in effect, provides the role of an equation of state. To find a suitable function, consider the expression for a Raleigh line given by

$$\frac{p_2 - p_1}{V_2 - V_1} = -\rho_2^2 (U_s - v_2)^2 \quad (2.167)$$

which connects some initial point 1 on a  $p - V$  Hugoniot to any other point 2 on the same  $p - V$  curve. Using this function, a plot of pressure versus particle speed can be produced that shows all possible states after passing through a single shock. Substituting the equation for the right-running experimental hugoniot and the jump condition for continuity, and after considerable manipulation results in

$$\Delta\sigma = \frac{\rho_1 \rho_2 C_0^2 (\rho_1 - \rho_2)}{[s(\rho_1 - \rho_2) + \rho_2]^2} \quad (2.168)$$

For the hydrostatic case, deviatoric stress will be 0. Assuming the reference pressure is also 0 and that the reference density is  $\rho_0$ , results in

$$P = \frac{\rho_0 \rho C_0^2 (\rho - \rho_0)}{[s(\rho_0 - \rho) + \rho]^2} \quad (2.169)$$

or expressed in terms of specific density as

$$P = \frac{C_0^2 (V_0 - V)}{[V_0(s - 1) - sV]^2} \quad (2.170)$$

For the elastic case using the experimental hugoniot, the effects of the deviatoric stress must be included. Assuming the reference deviatoric stress is 0 leaves

$$P = S_x + \frac{\rho_0 \rho C_0^2 (\rho - \rho_0)}{[s(\rho_0 - \rho) + \rho]^2} \quad (2.171)$$

or expressed in terms of specific density is

$$P = S_x + \frac{C_0^2 (V_0 - V)}{[V_0(s - 1) - sV]^2} \quad (2.172)$$

As described in the examples, the configuration of the test cases are the impact of two metal bars with properties given in Table 2.1. Their initial pressure, energy, and deviatoric stress are zero, i. e.  $p_1 = e_1 = S_{x_1} = 0.0$  and  $p_4 = e_4 = S_{x_4} = 0.0$  in both bars, and their initial densities are  $8930.0 \text{ Kg/m}^3$ . The velocities of the bars are given in the context of each test case.

### 2.3.1 Hydrostatic Test Case

See the example in Section 2.1.2 for details of this test case. The results of velocity vs. pressure, density, and energy are shown in Figures [6.1], [6.2], and [6.3], respectively. Table 2.5 shows a comparison of the results. Only state 2 is shown since state 3 is identical to state 2.

The results of this experiment indicate that the numerical algorithm is doing a very good job of capturing the fundamental physics of the problem.

Table 2.5: Exact vs. Computed Results for Hydrostatic case(State 2).

Parameter(Units)	Computed	Exact	Error
Velocity( $m/s$ )	0.0	0.000	0.0%
Pressure( $GPa$ )	3.652	3.653	0.0%
Density( $Kg/m^3$ )	9154.0	9153.866	0.0%
Energy( $J/Kg$ )	4991.0	5000.000	0.2%
Shock Vel.( $m/s$ )	-3994.0	-3989.000	0.1%

### 2.3.2 Elastic Solution using the Experimental Hugoniot.

See the example in Section 2.1.2 for details of this test case. The results of velocity vs. pressure, density, energy, and deviatoric stress are shown in Figures [6.4], [6.5], [6.6], and [6.7], respectively. The comparison between the exact solutions and the numerical solution are shown in Table 2.6.

This test case illustrates some oscillation particularly with the energy and the deviatoric stress near the impact point. However, the scheme is able to capture the correct values away from the oscillations.

### 2.3.3 Elastic Solution using the Mie-Grueneisen Equation of State

See the example in Section 2.1.2 for details of this test case. The results of velocity vs. pressure, density, energy, and deviatoric stress are shown in Figures [6.8], [6.9], [6.10], and [6.11], respectively. The comparison between the exact solutions and the numerical solution are shown in Table 2.7.

Table 2.6: Exact vs. Computed Results for Elastic case(State 2) using the Experimental Hugoniot.

Parameter(Units)	Computed	Exact	Error
Velocity( $m/s$ )	0.0	0.0	0.0%
Pressure( $MPa$ )	200.09	201.319	0.6%
Density( $Kg/m^3$ )	8952.65	8952.637	0.0%
Energy( $J/Kg$ )	50.0	49.9	0.1%
Deviatoric Stress( $MPa$ )	151.5837	-152.123	0.3%
Normal Stress( $MPa$ )	-353.1726	-353.1726	0.0%
Shock Vel.( $m/s$ )	-3994.0	-3967.8	0.5%

This test case is similar to the previous case in that both exhibit oscillations in deviatoric stress and energy near the impact point. However, like before the computed values are very close to the exact values away from the oscillations.

Table 2.7: Exact vs. Computed Results for Elastic case(State 2) using the Mie-Grueneisen Equation of State.

Parameter(Units)	Computed	Exact	Error
Velocity ( $m/s$ )	0.0	0.0000	0.0%
Pressure ( $MPa$ )	295.4	295.2880	0.0%
Density ( $Kg/m^3$ )	8948.9	8948.9250	0.0%
Energy ( $J/Kg$ )	49.9	50.0000	0.1%
Deviatoric Stress ( $MPa$ )	-127.0	-126.9700	0.0%
Shock Vel. ( $m/s$ )	-4741.4	-4718.6411	0.4%

### 2.3.4 Two-Wave Solution Using the Mie-Grueneisen Equation of State.

See the example given in Section 2.1.3 for details of this test case. The results of velocity vs. pressure, density, energy, and deviatoric stress are shown in Figures [6.12], [6.13], [6.14], and [6.15], respectively. The comparison between the exact solution and the numerical solution is shown in Table 2.8.

This test case has a much higher impact velocity than the previous case much as indicated by the higher error, although the oscillations are much better damped in proportion to the previous case.

Table 2.8: Exact vs. Computed Results for the Two-wave Shock using the Mie-Grueneisen Equation of State.

Parameter(Units)	State 1'			State 2		
	Computed	Exact	Error	Computed	Exact	Error
Velocity ( $m/s$ )	84.502	84.234	0.3%	0.0	0.000	0.0%
Pressure ( $MPa$ )	457.360	466.747	2.0%	3559.5	3558.695	0.0%
Density ( $Kg/m^3$ )	8959.270	8959.826	0.0%	9147.8	9147.919	0.0%
Energy ( $J/Kg$ )	120.369	124.272	3.1%	5199.0	5219.884	1.9%
Elastic Shock ( $m/s$ )	-4678.3	-4635.9538	0.9%			
Plastic Shock ( $m/s$ )				-3998.5	-4012.5352	0.4%

### 2.3.5 Single-Wave Plastic Solution using the Mie-Grueneisen Equation of State.

See the example given in Section 2.1.4 for details of this test case. The results of velocity vs. pressure, density, energy, and deviatoric stress as shown in Figures [6.16], [6.17], [6.18], and [6.19], respectively. The comparison between the exact solution and the numerical solution is shown in Table 2.9.

This solution exhibits some oscillation as the result of a very small undershoot of the velocity behind the shock. The undershoot causes the bar to unload elastically, then an oscillation sets up when the stress attempts to recover to the yield surface. One possible way to correct this behavior is to use a higher order temporal algorithm for the integration scheme.

Table 2.9: Exact vs. Computed Results for the Plastic Single-Wave response using the Mie-Grueneisen Equation of State.

Parameter(Units)	Computed	Exact	Error
Velocity ( $m/s$ )	0.0	0.000	0.0%
Pressure ( $GPa$ )	25.8	25.800	0.0%
Density ( $Kg/m^3$ )	10190.0	10189.950	0.0%
Energy ( $J/Kg$ )	180073.3	180458.200	0.2%
Deviatoric Stress ( $MPa$ )	-200.0	-200.000	0.0%
Shock Vel. ( $m/s$ )	-4249.0	-4135.954	2.0%



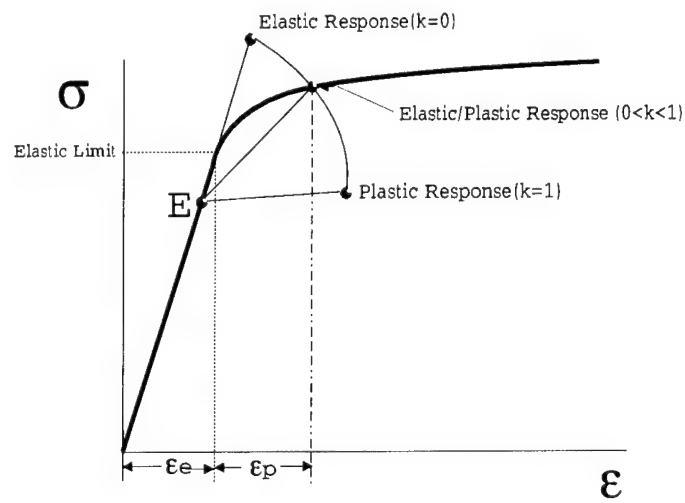


Figure 2.5: Figure illustrating the "Turning Method"

## Chapter 3

# Two-Dimensional Considerations

This chapter will present the equations of motion and the development of numerical algorithms to solve the equations of motion for hydrodynamic simulations. Two examples will be shown demonstrating the use of the algorithms.

### 3.1 Conservation Equations

In the absence of heat conduction and any sources the conservation equations for two-dimensional plane stress is written in the vector form as

$$\frac{\partial U}{\partial t} + \frac{\partial F}{\partial x} + \frac{\partial G}{\partial y} = 0 \quad (3.1)$$

or in the divergence form of

$$\nabla \cdot \bar{F} = 0 \quad (3.2)$$

where

$$\bar{F} = (U, F, G) \quad (3.3)$$

and

$$U = \begin{bmatrix} \rho \\ \rho u \\ \rho v \\ \rho e_T \end{bmatrix}, F = \begin{bmatrix} \rho u \\ \rho u^2 + p - S_x \\ \rho uv - S_{xy} \\ \rho ue_T + u(p - S_x) - vS_{xy} \end{bmatrix}, G = \begin{bmatrix} \rho v \\ \rho uv - S_{xy} \\ \rho v^2 + p - S_y \\ \rho ve_T + v(p - S_y) - uS_{xy} \end{bmatrix} \quad (3.4)$$

### 3.2 Constitutive Equations

The constitutive equations written to satisfy material frame indifference for plane strain is

$$\frac{D}{Dt} \begin{bmatrix} S_x \\ S_y \\ S_{xy} \\ \bar{\epsilon} \end{bmatrix} = \begin{bmatrix} S_{xy} \left( \frac{\partial u}{\partial y} - \frac{\partial v}{\partial x} \right) + 2G \left( \frac{2}{3} \frac{\partial u}{\partial x} - \frac{1}{3} \frac{\partial v}{\partial y} - \frac{3}{2} \beta \frac{S_x}{\bar{\sigma}^2} \phi_{xy} \right) \\ S_{xy} \left( \frac{\partial v}{\partial x} - \frac{\partial u}{\partial y} \right) + 2G \left( \frac{2}{3} \frac{\partial v}{\partial y} - \frac{1}{3} \frac{\partial u}{\partial x} - \frac{3}{2} \beta \frac{S_y}{\bar{\sigma}^2} \phi_{xy} \right) \\ \frac{1}{2} (S_y - S_x) \left( \frac{\partial u}{\partial y} - \frac{\partial v}{\partial x} \right) + G \left( \frac{\partial v}{\partial x} + \frac{\partial u}{\partial y} - \frac{3}{2} \beta \frac{S_{xy}}{\bar{\sigma}^2} \phi_{xy} \right) \\ \beta \frac{\phi_{xy}}{\bar{\sigma}^2} \end{bmatrix} \quad (3.5)$$

where

$$\phi_{xy} = S_x \frac{\partial u}{\partial x} + S_y \frac{\partial v}{\partial y} + S_{xy} \left( \frac{\partial u}{\partial y} + \frac{\partial v}{\partial x} \right) \quad (3.6)$$

The conservation equations (Section 3.1) solved with the constitutive equations and closed with an equation of state (Section 2.1.5) form the complete equations of motion for hydrodynamics.

### 3.3 Integration of the Conservation Equations

The method of Integration follows closely with that developed in Section 2.2 for the case of uniaxial strain. Assuming two space dimensions Eq.[2.130] is written as

$$\oint_S (\bar{F} \cdot \hat{\eta}) dS = \oint_S (U \hat{\eta}_t + F \hat{\eta}_x + G \hat{\eta}_y) dS = 0 \quad (3.7)$$

Expanding the terms in the expression above we have

$$\mathcal{F}(\mathbf{U}, \hat{\eta}) = \bar{F} \cdot \hat{\eta} = \begin{bmatrix} \rho U_n \\ \rho u U_n + (p - S_x) \hat{\eta}_x - S_{xy} \hat{\eta}_y \\ \rho v U_n - S_{xy} \hat{\eta}_x + (p - S_y) \hat{\eta}_y \\ \rho e_T U_n + [u(p - S_x) - v S_{xy}] \hat{\eta}_x + [v(p - S_y) - u S_{xy}] \hat{\eta}_y \end{bmatrix} \quad (3.8)$$

where  $U_n \equiv (\hat{\eta}_t + u \hat{\eta}_x + v \hat{\eta}_y)$ .

The continuum is discretized using an unstructured grid system where the field parameters are stored at the vertices of the grid. A control volume (c.v.) is constructed about each vertex using the dual medium grid as shown in Figure [3.1].

Summing Eq.[3.8] on all faces and setting the total flux of the time-space slab to zero requires that

$$U^{n+1} A^{n+1} - U^n A^n + \sum_{i=1}^{n_s} \mathcal{F}_i(U, \bar{\eta}) |\bar{\eta}| = 0 \quad (3.9)$$

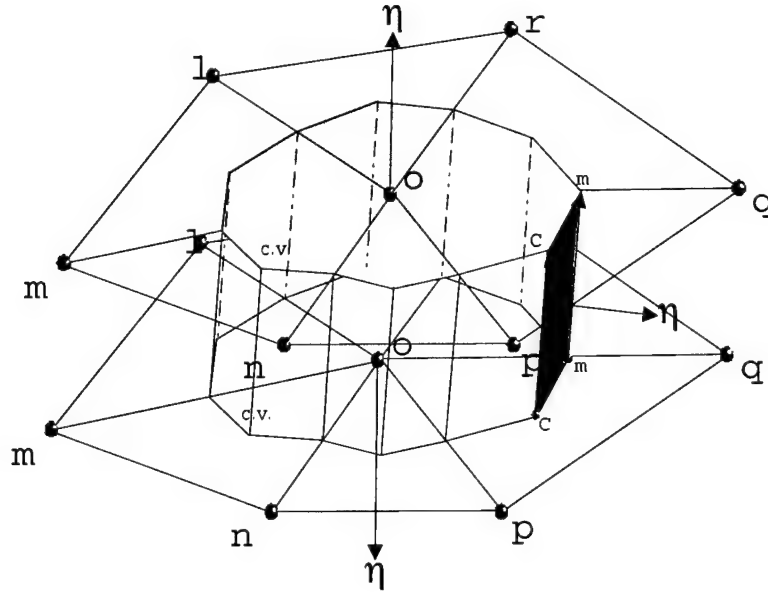


Figure 3.1: The control volume using a dual medium grid.

where  $n_s$  is the number of lateral sides on the control volume. For each edge connecting the center node "o", and each neighboring vertex, two flux evaluations are required corresponding to the two segments connecting the center of the adjacent cells "c" to the center of the edge "m". Although other control volumes can be constructed such as connecting the center of the cells directly, the dual medium has been shown to provide the best results, particularly when the cell structure is skewed [22].

A second order scheme in time and space is formed by a two-step explicit integration algorithm. The predictor step is a simple Euler integration derived by solving Eq.[3.9] for the term at the " $n + 1$ " level or

$$U^* A^* = U^n A^n + \Delta U^n \quad (3.10)$$

where

$$\Delta U^n = - \sum_{i=1}^{n_s} \mathcal{F}_i^n(U, \hat{\eta}) |\hat{\eta}| \quad (3.11)$$

The corrector phase is calculated as

$$U^{n+1} A^{n+1} = U^n A^n + \frac{1}{2} [\Delta U^* - \Delta U^n] \quad (3.12)$$

where

$$\Delta U^* = - \sum_{i=1}^{n_s} \mathcal{F}_i^*(\mathbf{U}, \hat{\eta}) |\bar{\eta}| \quad (3.13)$$

The lateral flux component  $\mathcal{F}(\bar{U}, \hat{\eta})$  is needed at the middle of the edge segment “m”, yet the field parameters are stored at the vertices. There are many methods which can be used to estimate the flux at the center of the edge, but one of the most popular is the class of upwind methods. Reference [22] suggests a method based on an approximate Riemann method where

$$\mathcal{F}(\mathbf{U}, \hat{\eta})|_o = \sum_{i=1}^{n_s} \frac{1}{2} |\bar{\eta}| \left( \mathcal{F}(\mathbf{U}_0, \hat{\eta}_0) + \mathcal{F}(\mathbf{U}_i, \hat{\eta}_i) - \left| \frac{\partial \mathcal{F}(\mathbf{U}_m, \hat{\eta}_m)}{\partial \mathbf{U}} \right| (\mathbf{U}_i - \mathbf{U}_0) \right) \quad (3.14)$$

The absolute value sign around the derivative indicates some form of eigenvalue decomposition and normalization. This procedure requires not only the eigenvalue calculation, but also similarity transformation matrices. However, the complexity of this operation is not warranted. The sound speed is much larger than the local particle velocity and is therefore dominated by the  $u + c$  eigenvalue. As a result, the absolute value operation in Eq.[3.14] is replaced with a scalar velocity  $\alpha$  which satisfies a positivity condition on the eigenvalues where

$$\alpha > \frac{1}{2} |\lambda_i|_{max} \quad (3.15)$$

where

$$\lambda_i : \text{eigenvalues of } \left. \frac{\partial \mathcal{F}(\mathbf{U}, \hat{\eta})}{\partial \mathbf{U}} \right|_m \quad (3.16)$$

The eigenvalue calculation is given in Section [2.2.3]. Substituting  $\alpha$  in Eq.[3.14] leaves

$$\mathcal{F}(\mathbf{U}, \hat{\eta})|_o = \sum_{i=1}^{n_s} \frac{1}{2} |\bar{\eta}| \left( \mathcal{F}(\mathbf{U}_0, \hat{\eta}_0) + \mathcal{F}(\mathbf{U}_i, \hat{\eta}_i) - \alpha (\mathbf{U}_i - \mathbf{U}_0) \right) \quad (3.17)$$

### 3.4 Integration of the Constitutive Equations

The fundamental concept of integrating the constitutive equations [3.5] is to replace the partial derivatives with finite volume expressions, then applying some standard technique for integrating the resulting first-order Ordinary Differential Equation. The integration technique for two-dimensions is the same as shown in Section [3.2] and will not be repeated here.

### 3.5 Results for Two-Dimensional Plane Strain

The concepts explored in the case of uniaxial strain were extended into two-dimensions primarily to understand if the numerical algorithms would extend into multi-dimensions as expected. Two simple test cases are presented that illustrate reasonable qualitative plastic behavior, though the results were not validated.

The first test case was a finite length bar impacting a non-deformable surface at 1000  $m/s$  (See Figure [6.20]). The boundary condition on the left wall was zero horizontal deflection, thereby simulating a centerline. The boundary condition imposed on the bottom surface was no vertical deflection. The right and top boundaries were free to deform as calculated and imposed a zero stress boundary. Ideally, the boundary condition should be zero surface traction, i. e.,  $n_j \sigma_{ji} = 0$  but the details of the implementation were never explored. In addition, the nodes on the interior of the simulation were moved during each time step such that LaPlace's solution was approximately satisfied at each time step, or

$$\nabla^2 x + \nabla^2 y = 0 \quad (3.18)$$

This adaptivity provides a smooth variation of the interior grid nodes to large deformations at the boundary. Similar results were obtained if the interior nodes were allowed to follow the particle velocity rate.

The second test case is identical to the first test case except a notch was included on the output boundary. The initial configuration is shown in Figure [6.21], and the deformed geometry is shown magnified in Figure [6.22].

Neither of these two test cases were evaluated in any detail other than to observe that the results indicated basic plastic response (i.e. mushrooming of the base) with an elastic rebound which was observed. The boundary conditions were not accurate and therefore would never compare favorably with data.

## Chapter 4

# Conclusion

The overall conclusion is an Eulerian form of the equations of motion for hydrodynamics can be used to numerically simulate a wide range of impact velocities with great accuracy with little oscillation in the solution. The best observed upwind technique to solve these equations is the ENO technique which produces the sharpest shocks with the least amount of smearing. However, very high orders of accuracy in both time and space are necessary to achieve accurate solutions without oscillations, although correct jump conditions can be achieved in the presence of oscillations with lower order solutions. Small errors in velocity, particularly shock undershoots, can cause the deviatoric stress to unload generating large errors and oscillations in the stress field.

Exact solutions to impact problems using multiple materials can be produced using the Mie-Grueneisen Equation of State, though not all the solutions are explicit and must be solved using numerical techniques to handle algebraic non-linearity.

It is not desirable to solve the conservation equations and the constitutive equations as a coupled set of partial differential equations. It was illustrated that there were no discovered divergence forms that produced eigenvectors which remain bounded, and therefore retained its hyperbolic character. Secondly, no forms could be found which produced any different eigenvalues beyond that of the conservative system, therefore no gain would be attributed to the coupling. Perhaps the strongest argument is that some of the exact solutions demonstrate that the solution to the conservative equations were dependent only on the normal stress, and not on the individual stress components<sup>1</sup>. Therefore, it would not make physical sense to couple the conservative and constitutive equations when the physics are not coupled.

---

<sup>1</sup>As an example, the solution for the hydrostatic and the elastic solution produce the same normal stress independent of the choice of stress model

## Chapter 5

# Recommendations

The research effort in examining the potential of using the Eulerian form of the equations of motion coupled with an upwind solution methodology is a success. The result of the numerics illustrates an exceptional capability to capture the correct jump conditions across shocks without the use of artificial dissipation to maintain stability. Although shocks are reasonably sharp using the WENO integration algorithm, the numerical solution for very high impact velocities exhibits a tendency for the deviatoric stress to unload in the presence of small velocity undershoots downstream of the shock. This defect in stress in turn corrupts the calculation of plastic strain. This effect may be minimized by using a scheme with fourth-order or higher accuracy in time (the current scheme is fifth order accurate in space, and second order in time).

Another strategy which needs to be examined is the level of improvement in the solution accuracy that could be realized by applying upwind techniques to the equations of motion cast in the Lagrange form. Simple numerical experiments using central difference approximations indicate the ability to capture shocks sharply, although artificial diffusion has to be applied to maintain stability, which taints the accuracy of the solution. Upwind techniques should further refine the shock without the explicitly added artificial viscosity resulting in higher accuracy.

Much work is yet to be done on both the numerical model and the validation of the two-dimensional computer code. The current implementation needs to be expanded to include the axisymmetric form for validation against the Taylor impact experimental data.



## Chapter 6

# Additional Figures

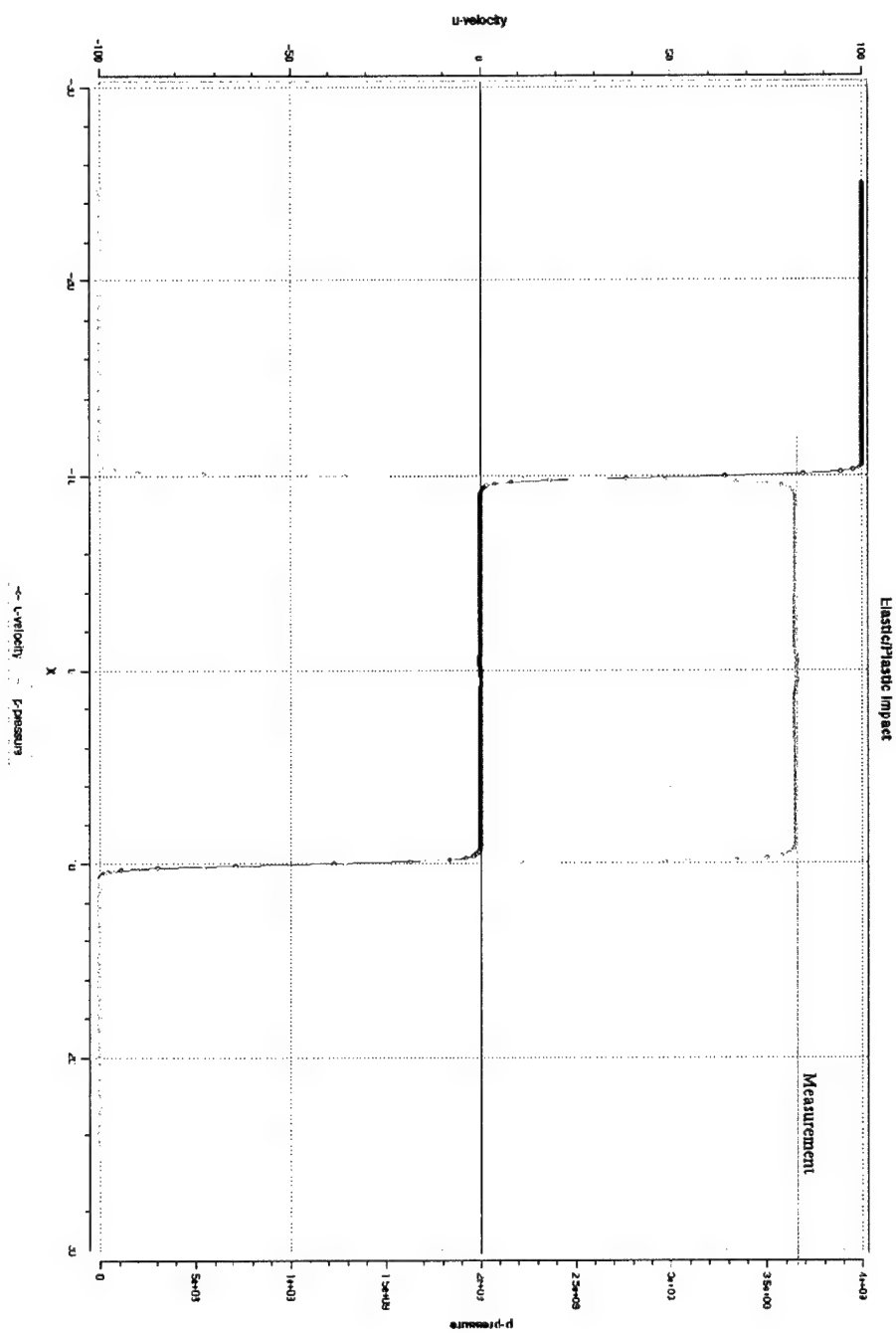


Figure 6.1: Pressure for hydrostatic test case.

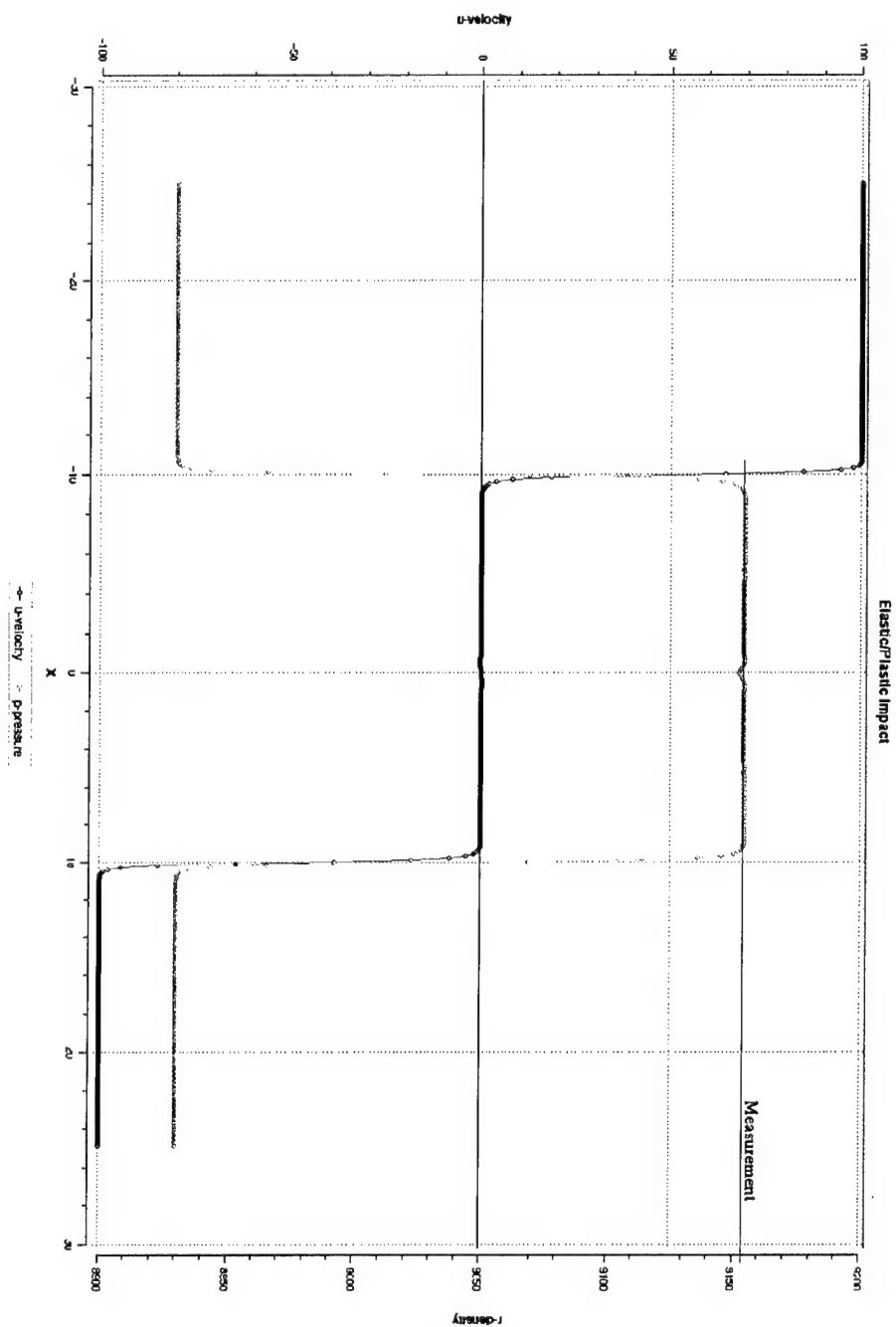


Figure 6.2: Density for hydrostatic test case.

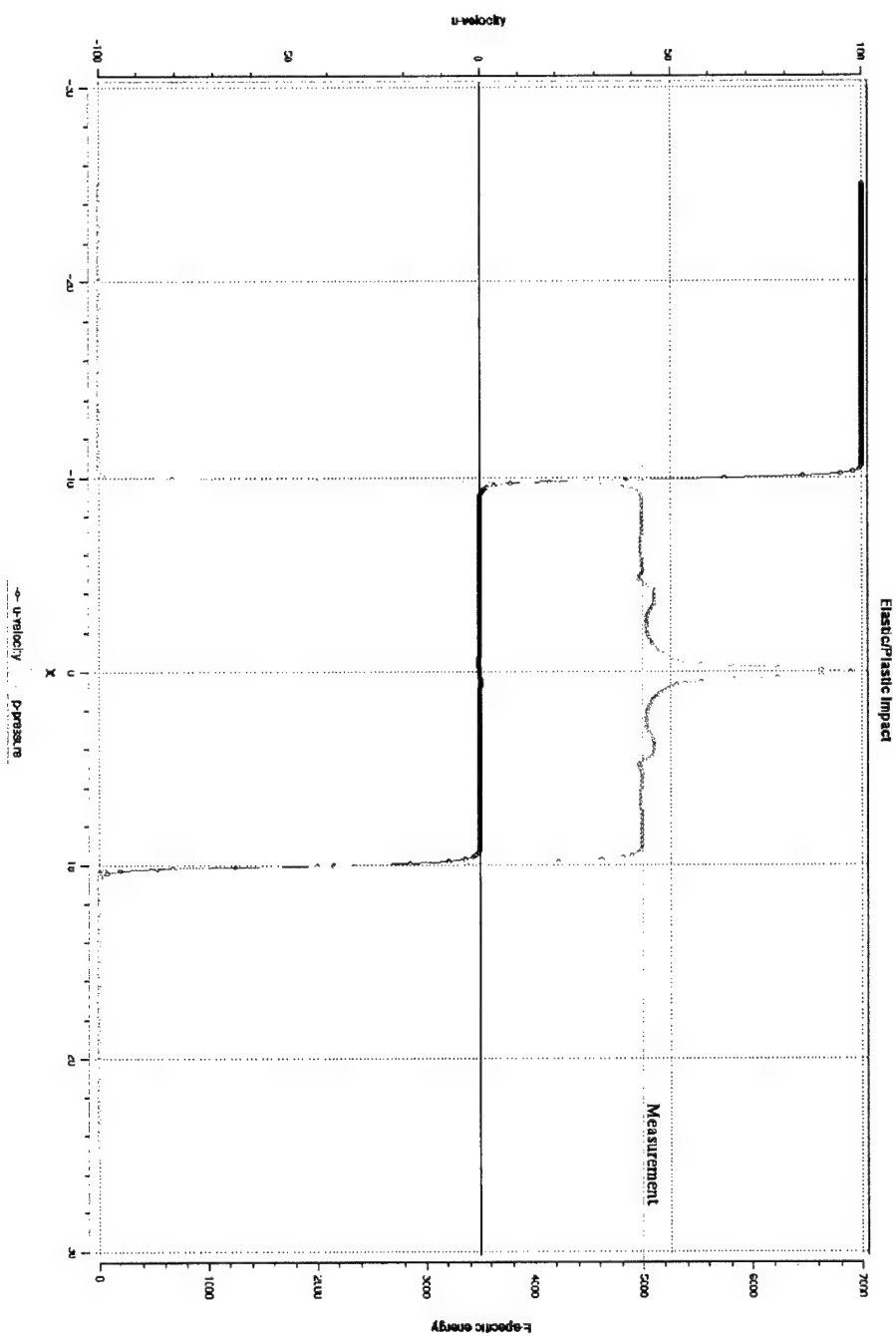


Figure 6.3: Energy for hydrostatic test case.

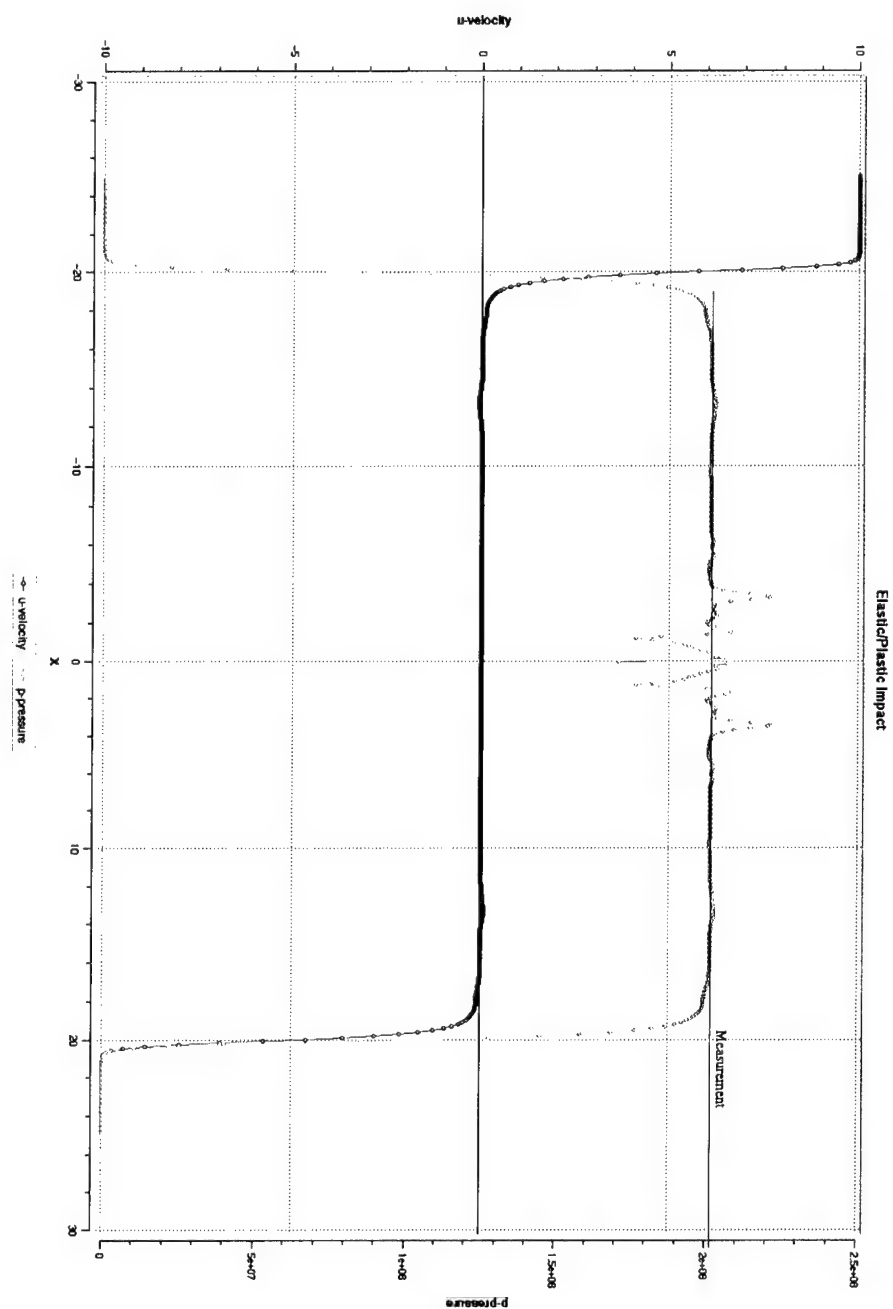


Figure 6.4: Pressure for elastic test case using the Experimental Hugoniot.

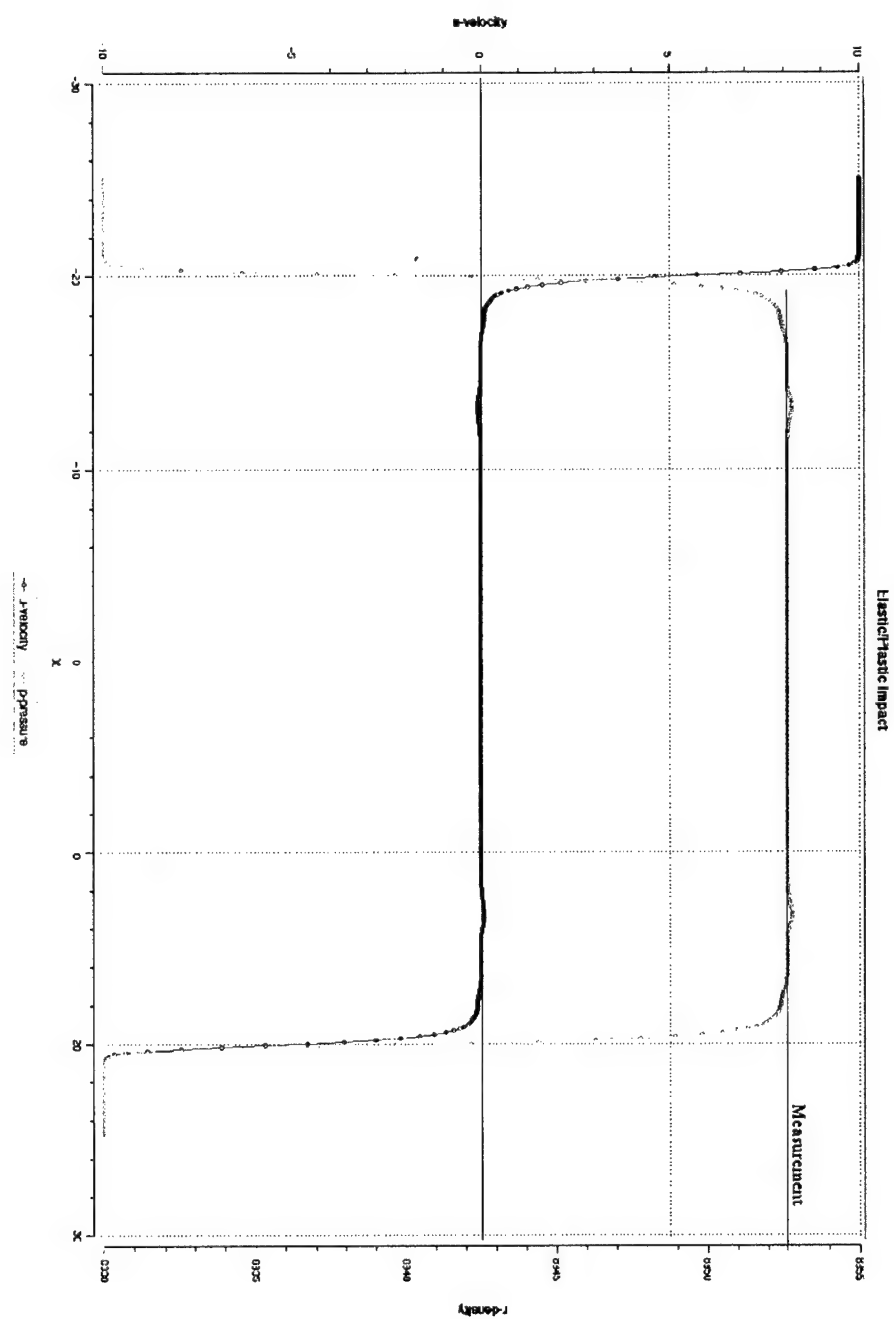


Figure 6.5: Density for elastic test case using the Experimental Hugoniot.

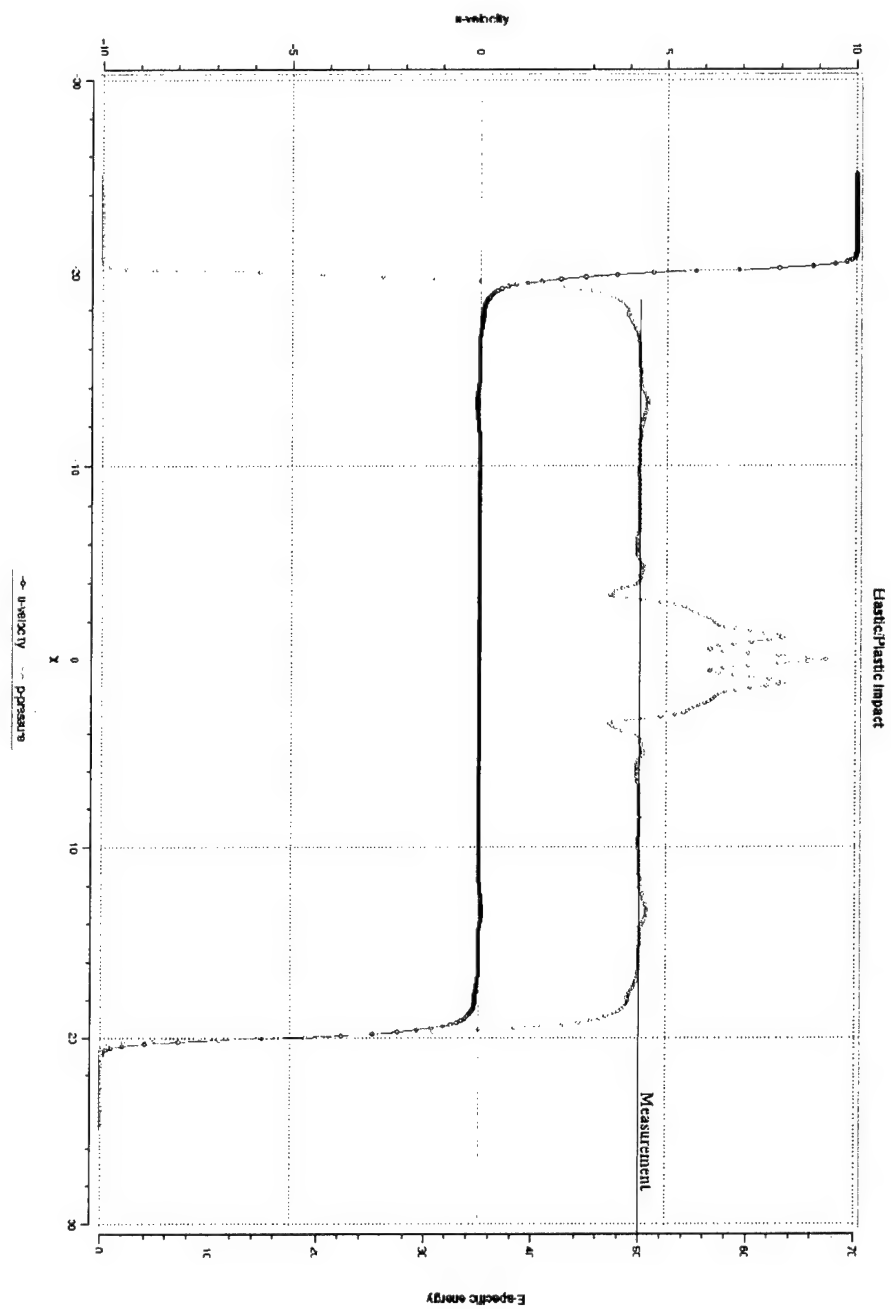


Figure 6.6: Energy for elastic test case using the Experimental Hugoniot.

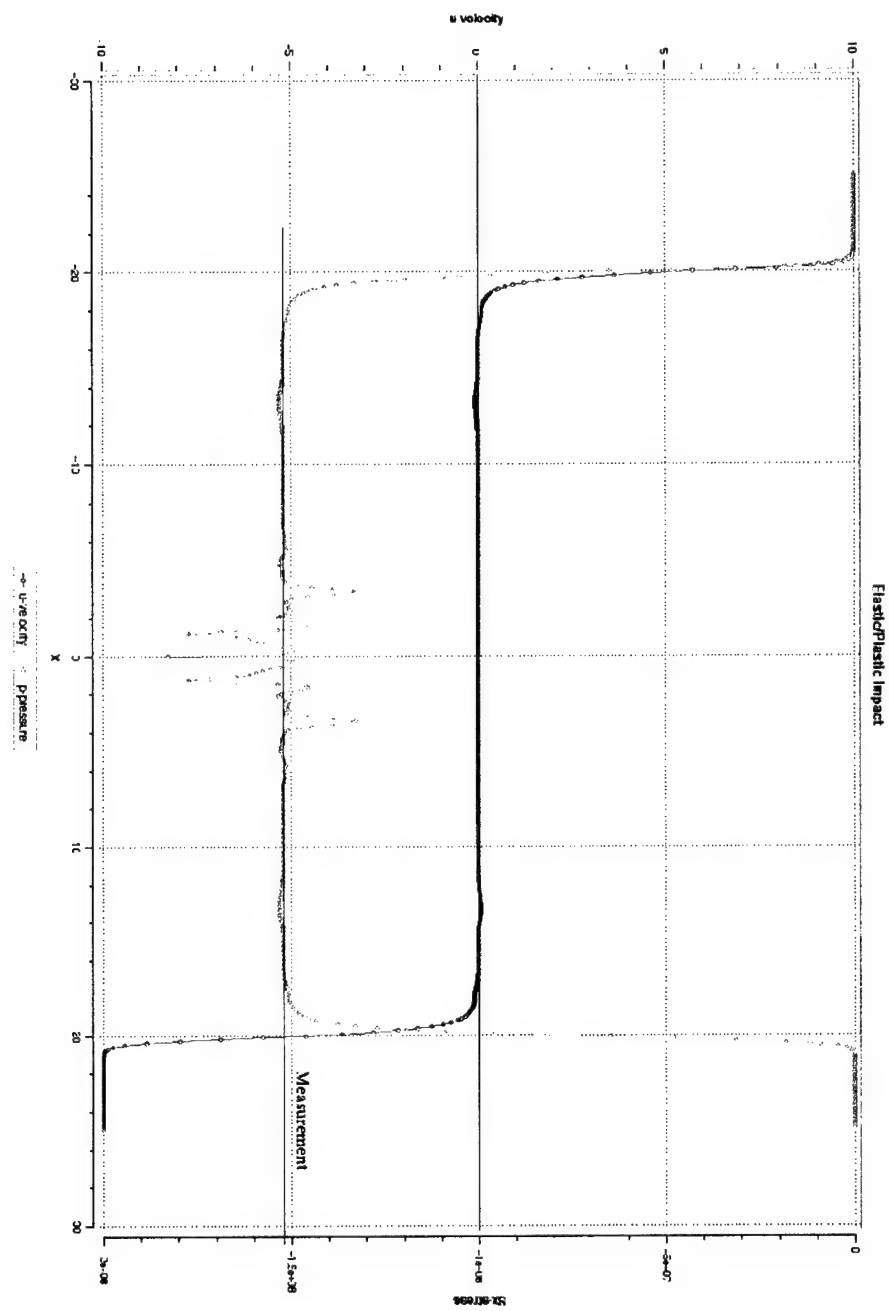


Figure 6.7: Deviatoric Stress for elastic test case using the Experimental Hugoniot.





Figure 6.8: Pressure for elastic test case using the Mie-Grueneisen equation of state.

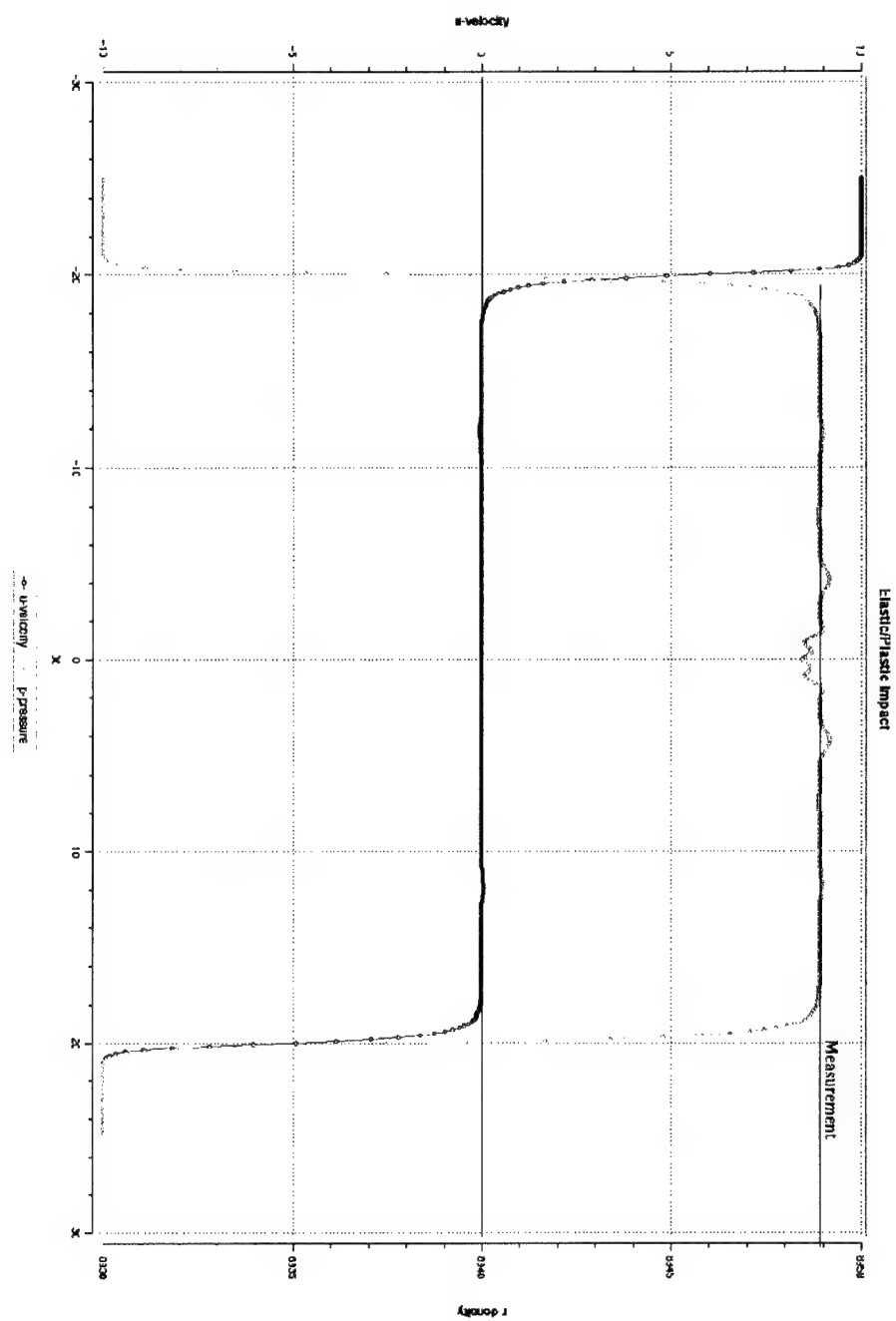


Figure 6.9: Density for elastic test case using the Mie-Grueneisen equation of state.

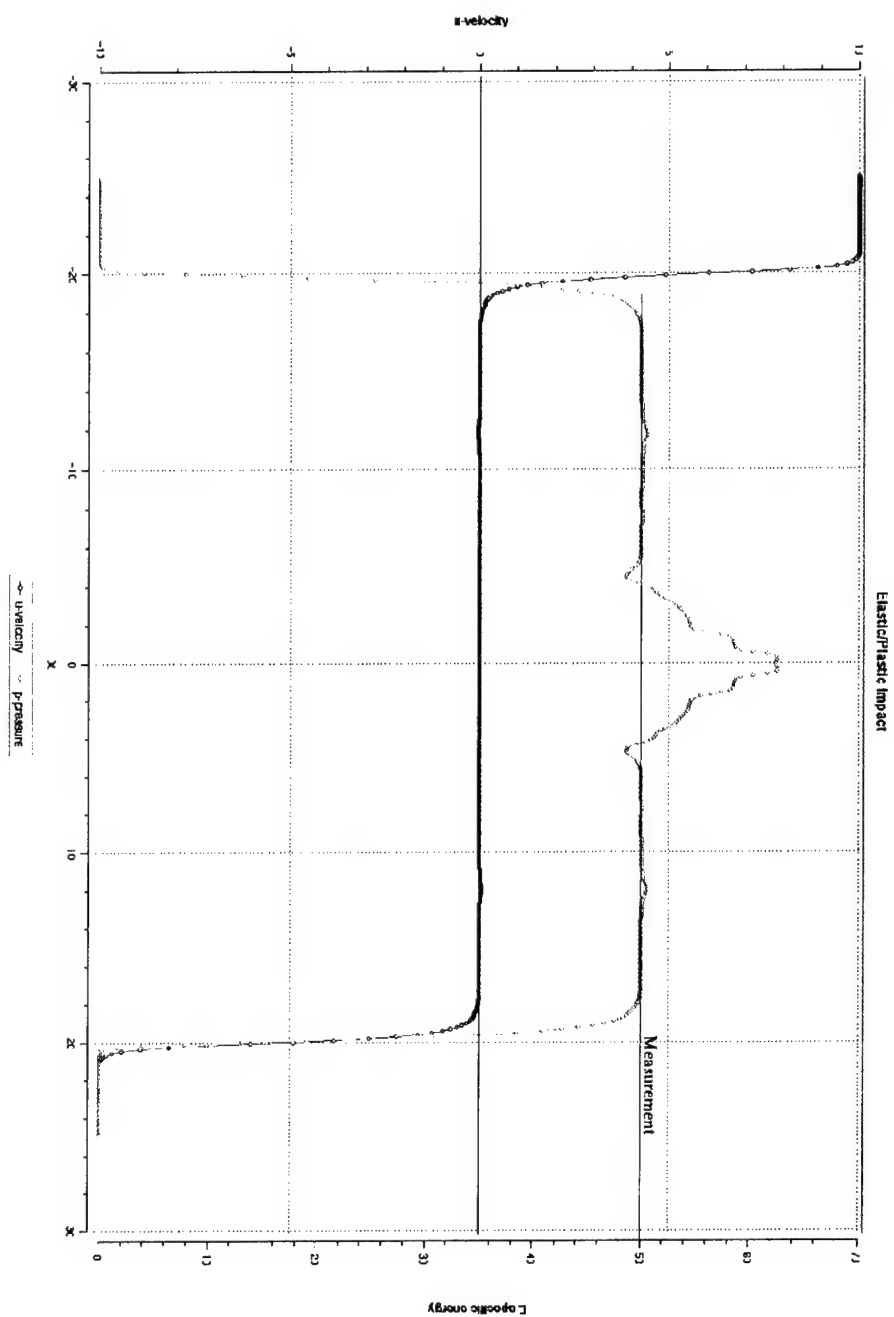


Figure 6.10: Energy for elastic test case using the Mie-Grueneisen equation of state.

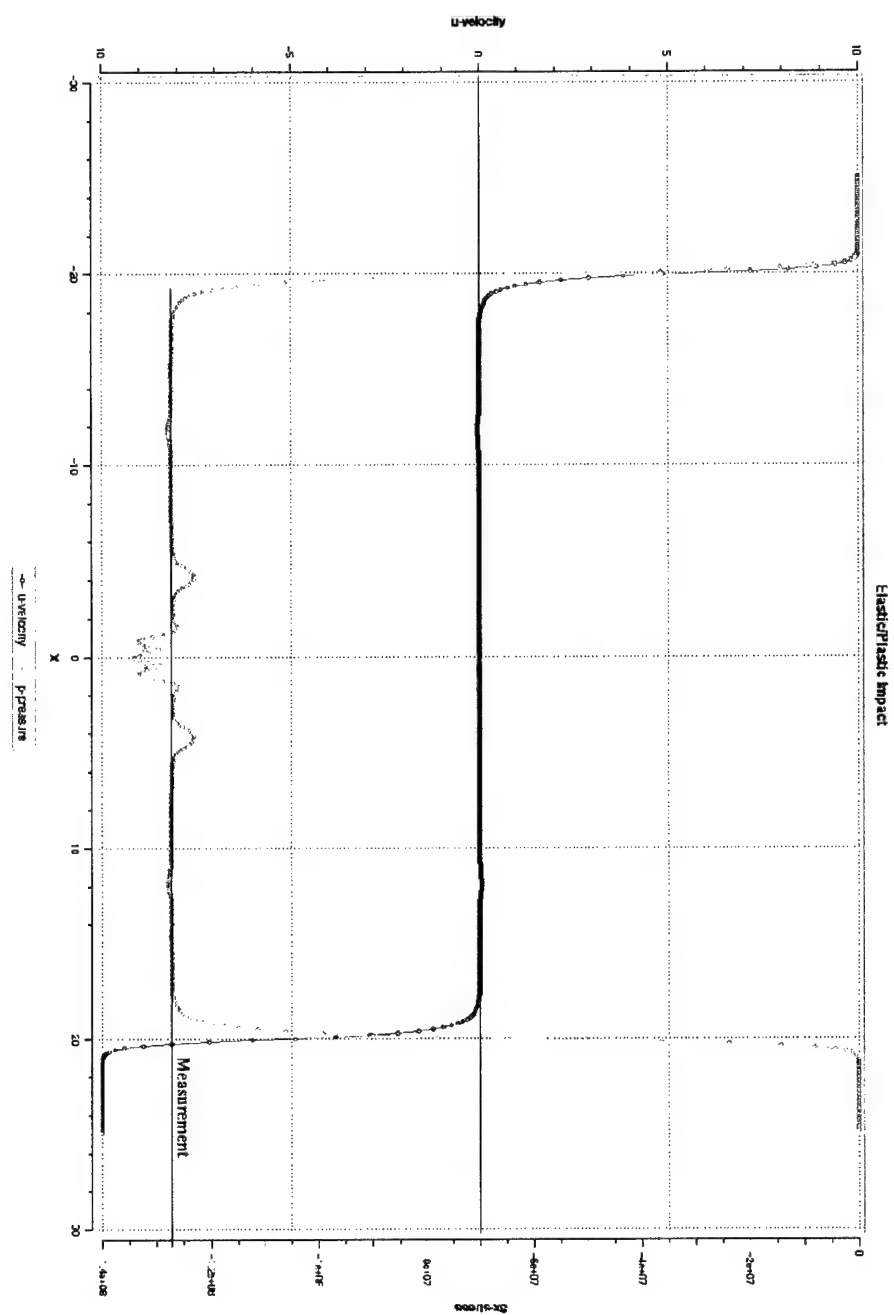


Figure 6.11: Deviatoric stress for elastic test case using the Mie-Grueneisen equation of state.

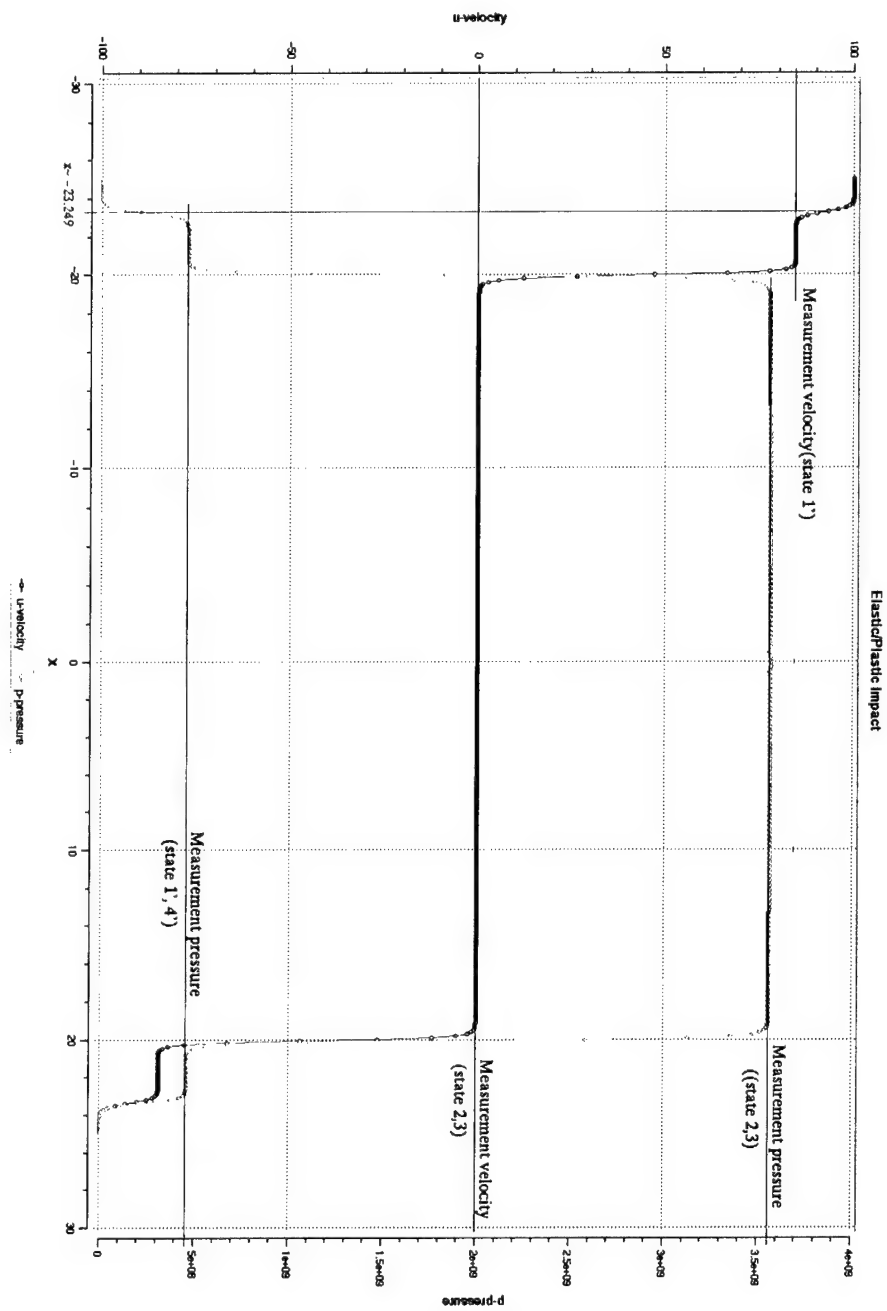


Figure 6.12: Pressure for two-wave test case using the Mie-Grueneisen equation of state.

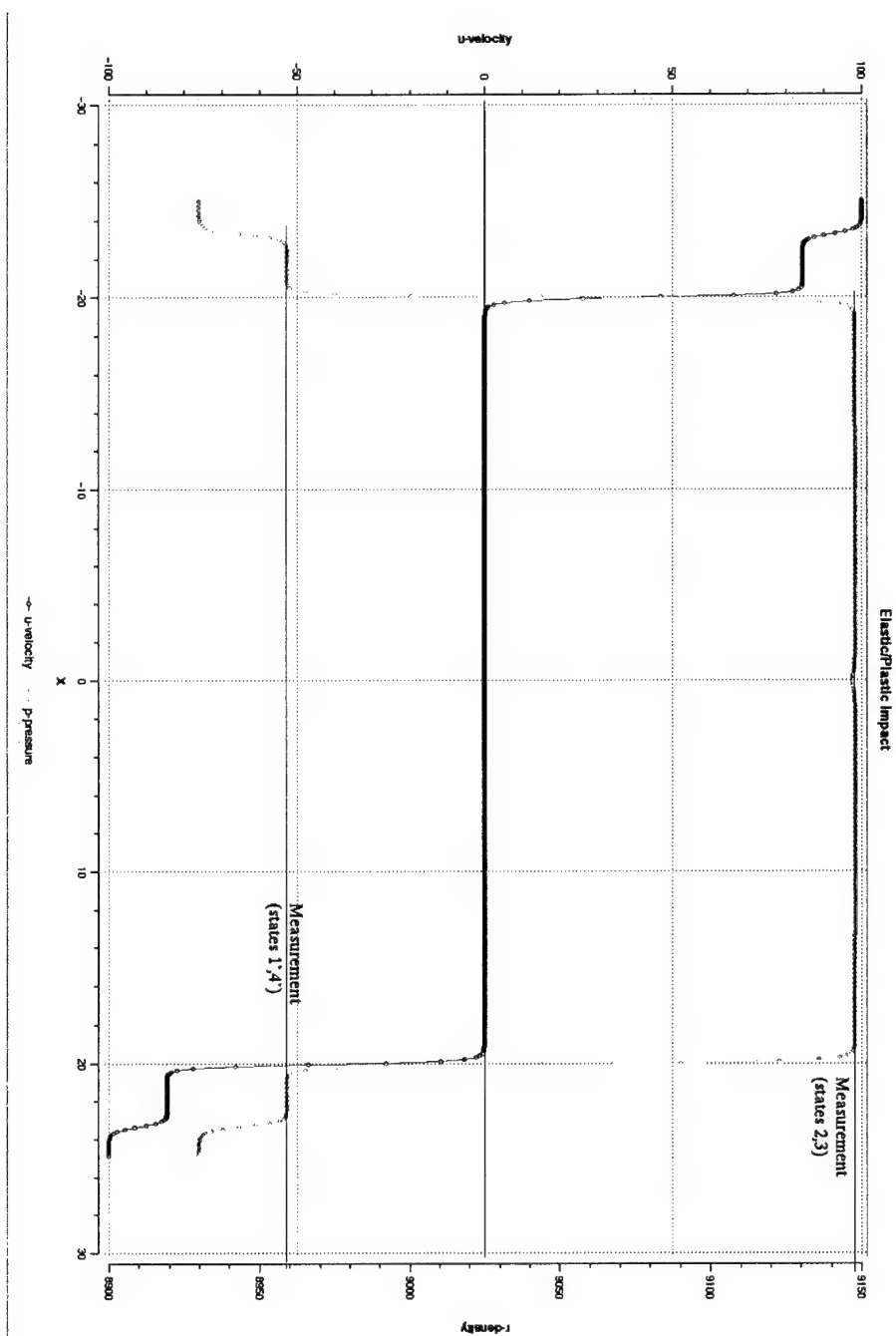


Figure 6.13: Density for two-wave test case using the Mie-Grueneisen equation of state.

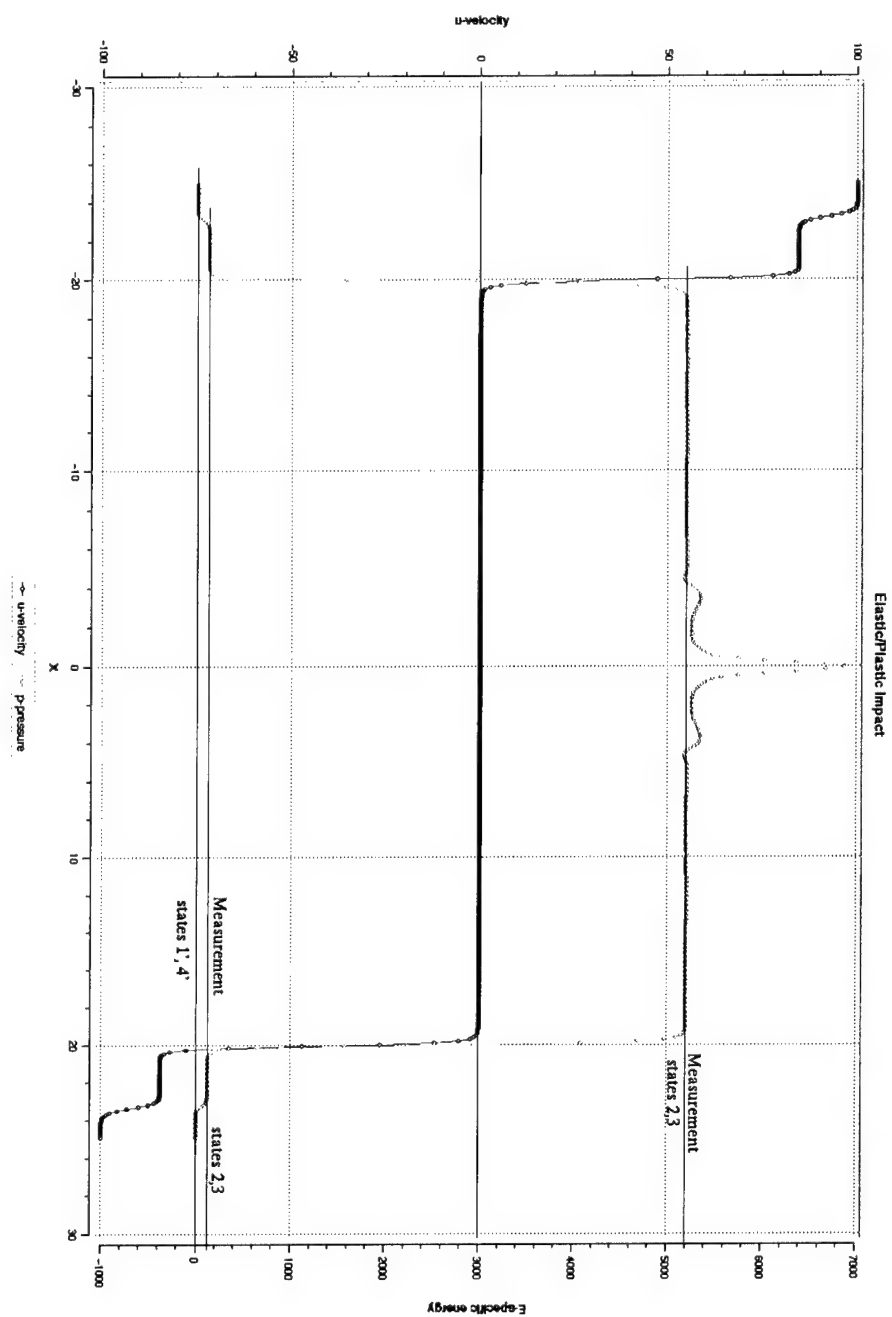


Figure 6.14: Energy for two-wave test case using the Mie-Grueneisen equation of state.

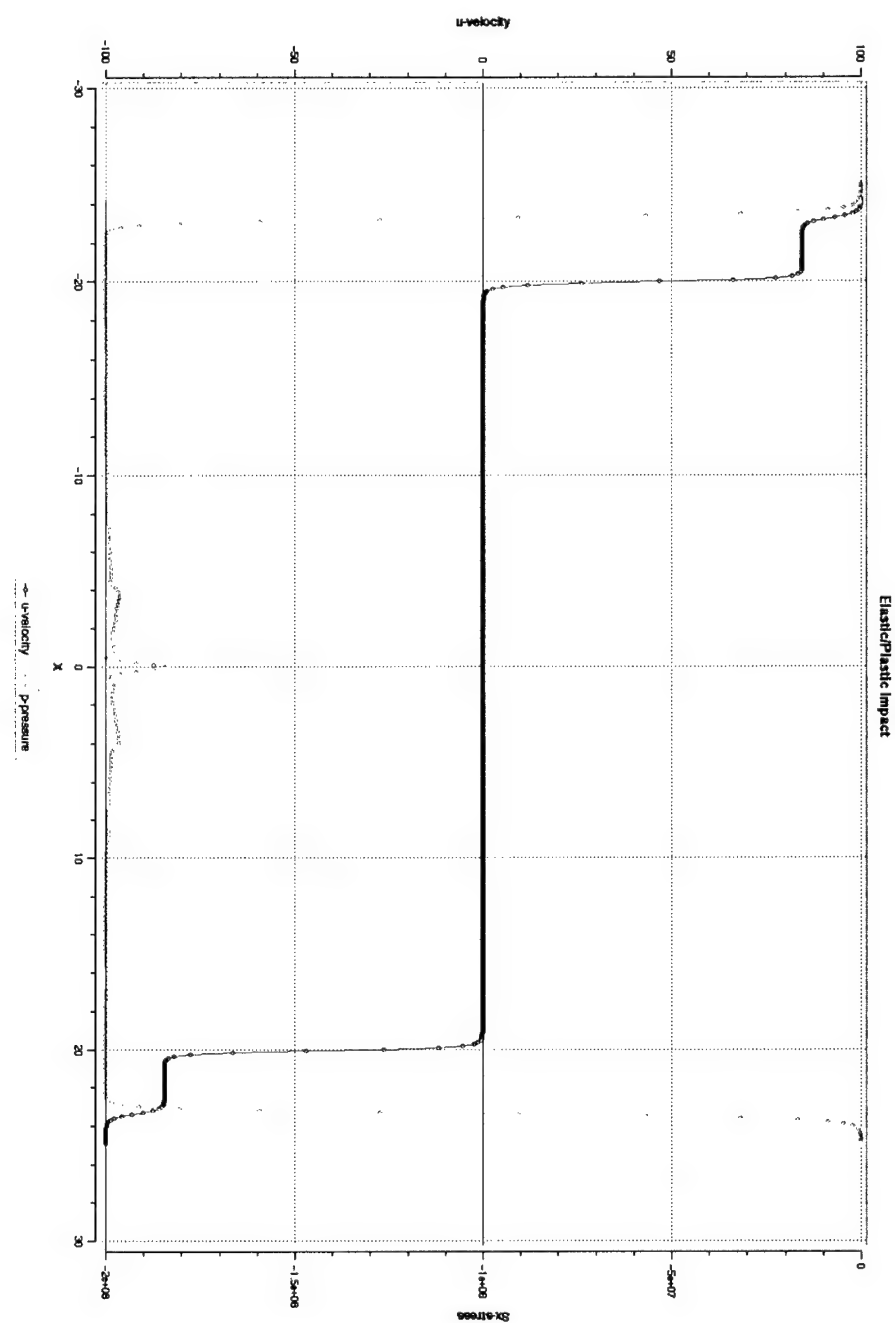


Figure 6.15: Deviatoric stress for two-wave test case using the Mie-Grueneisen equation of state.





Figure 6.16: Pressure for single-wave test case using the Mie-Grueneisen equation of state.

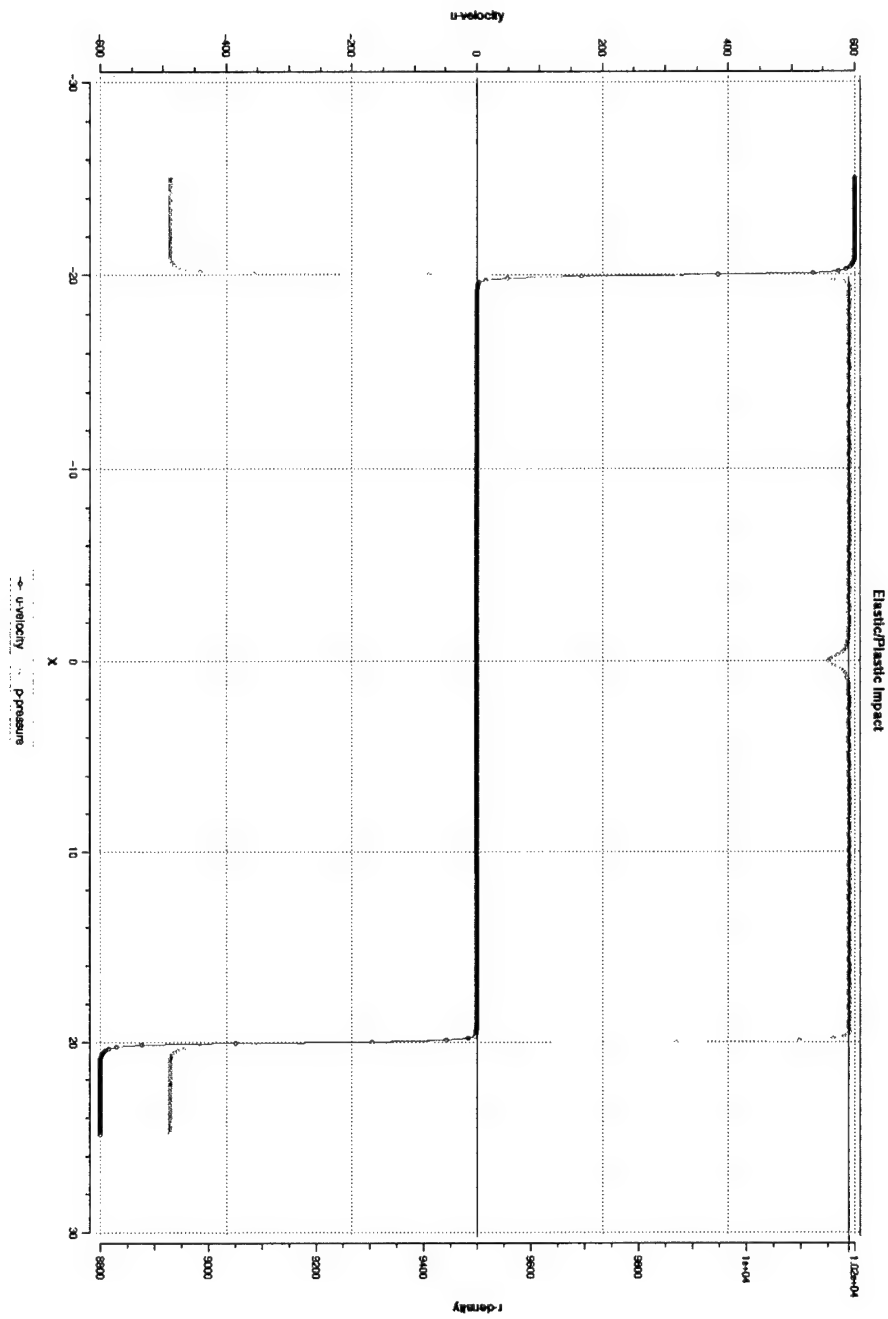


Figure 6.17: Density for single-wave test case using the Mie-Grueneisen equation of state.

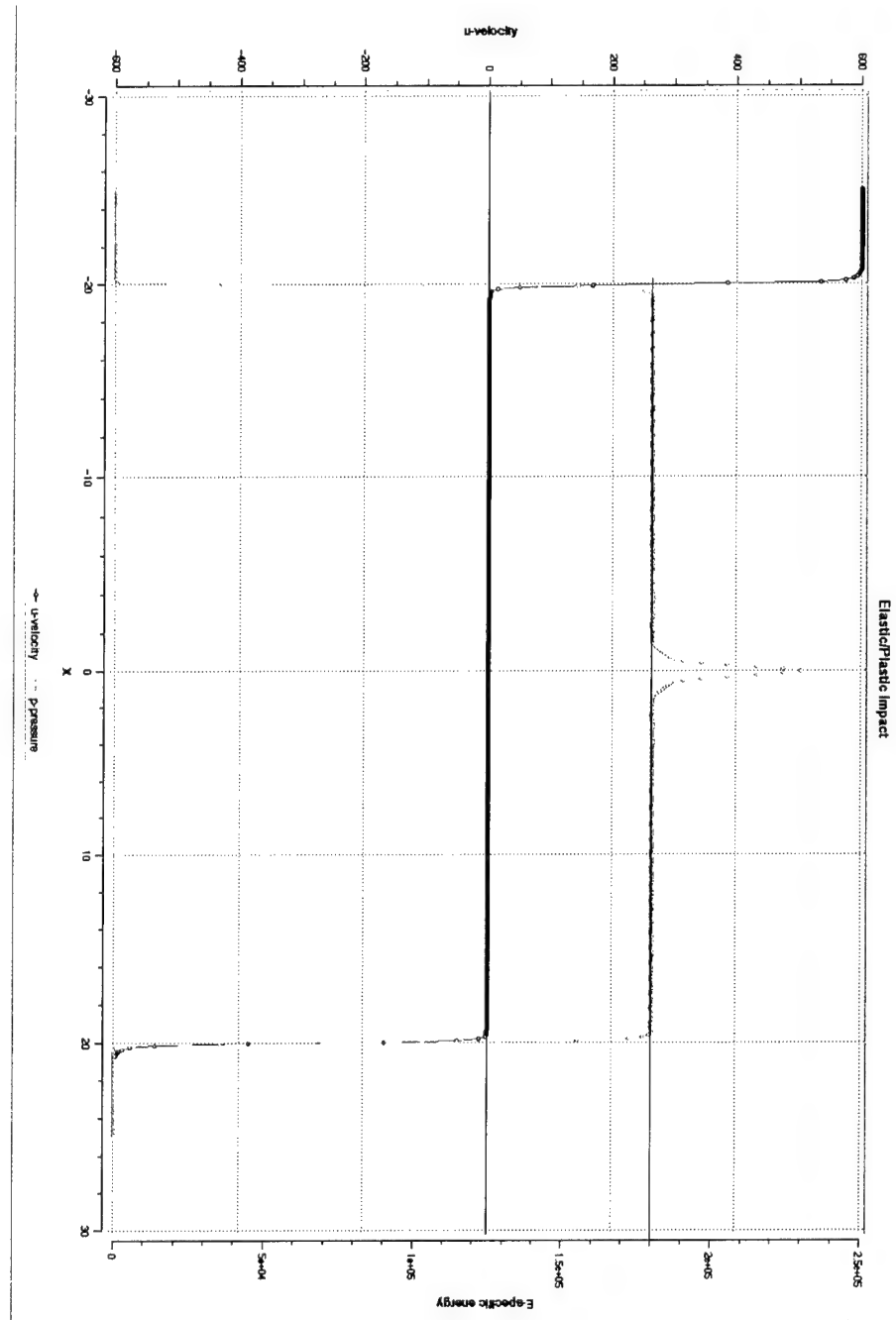


Figure 6.18: Energy for single-wave test case using the Mie-Grueneisen equation of state.

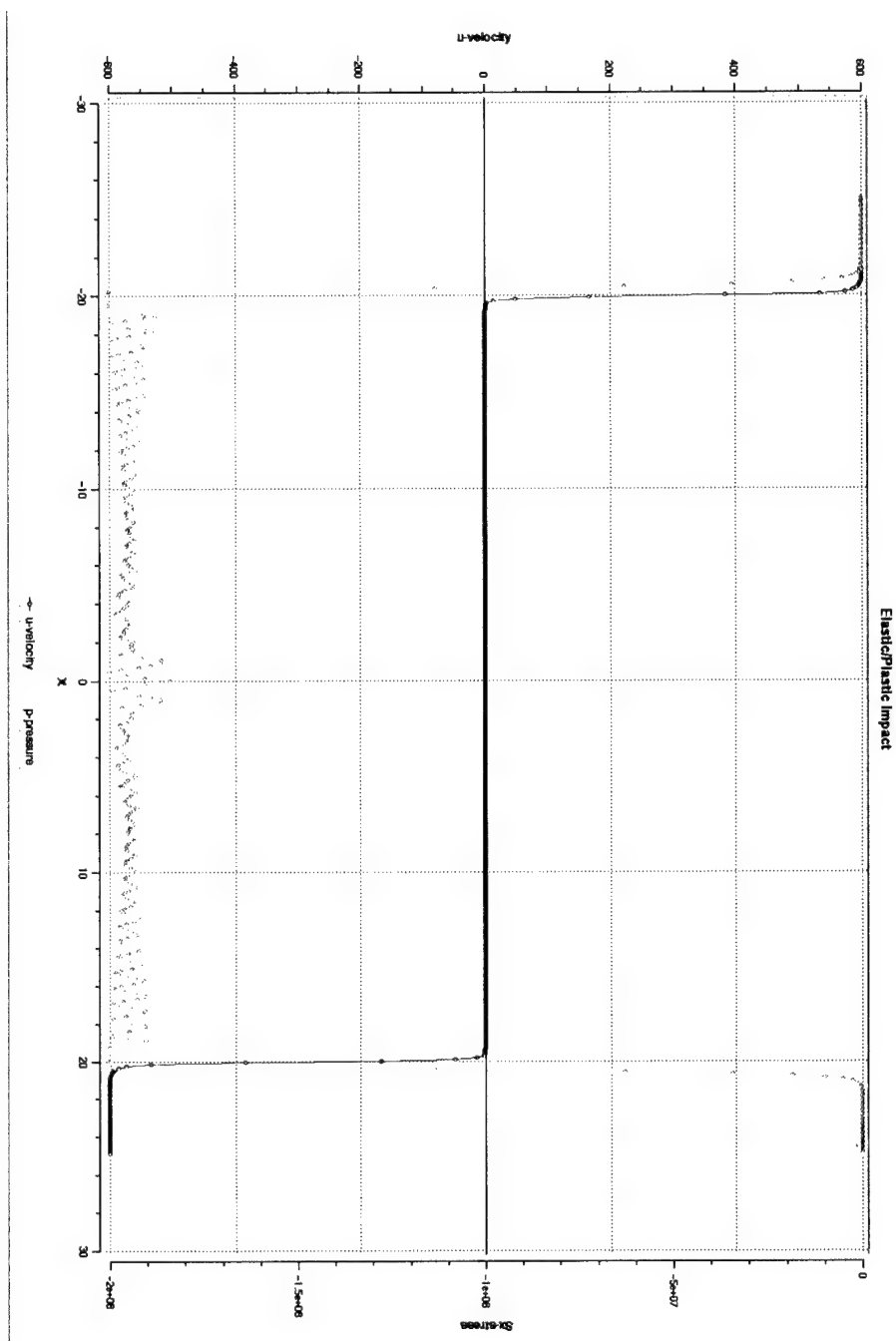
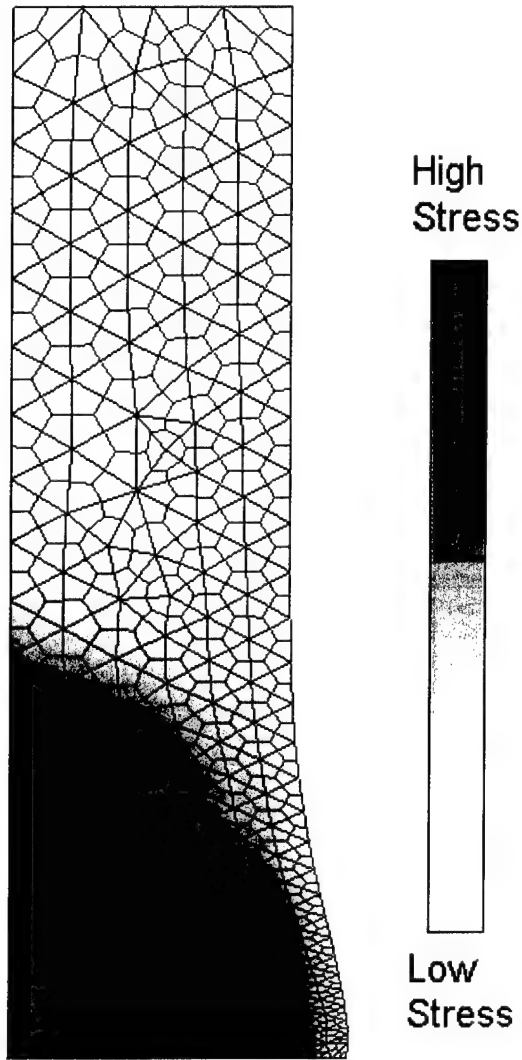


Figure 6.19: Deviatoric stress for single-wave test case using the Mie-Grueneisen equation of state.



Copper Bar  
Impact Vel. 1000 m/s

Figure 6.20: Pressure for impact of Copper Bar at 1000 m/s.

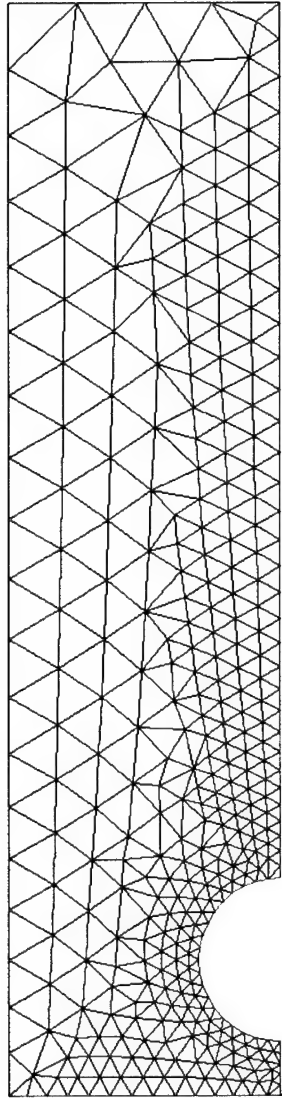


Figure 6.21: Initial Configuration of notched bar.

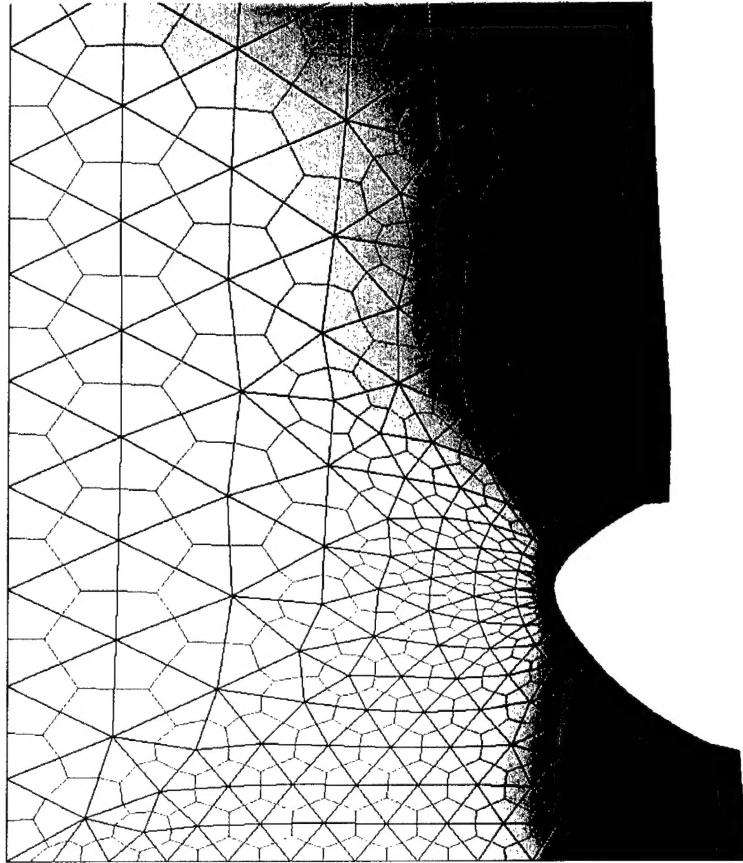


Figure 6.22: Deformed Configuration of notched bar with Pressure.

# Bibliography

- [1] Benson, David J., "Computational Methods in Lagrangian and Eulerian Hydrocodes" *Computer Methods in Applied Mechanics and Engineering*, **99**, (1992) 235-394.
- [2] Lawrence E. Malvern, *Introduction to the Mechanics of a Continuous Medium*. Prentice -Hall, Inc., 1969.
- [3] Rutherford Aris. *Vectors, Tensors, and the Basic Equations of Fluid Mechanics*. Dover Publications, Inc., 1962.
- [4] George E. Mase. *Continuum Mechanics*. Schaum's Outline Series. McGrawHill, Inc., 1970.
- [5] J. L. Synge and A. Schild. *Tensor Calculus*. Dover Publications, Inc., 1949.
- [6] Ronald P. Fedkiw, Barry Merriman, and Stanley Osher, "Simplified Discretization of Systems of Hyperbolic Conservation Laws Containing Advection Equations," <ftp://ftp.math.ucla.edu/pub/camreport/cam98-16.ps.gz>.
- [7] P.D. Thomas, and C.K. Lonbard, "Geometric Conservation Law and Its Application to Flow Computations on Moving Grids," AIAA Journal VOL. 17, NO. 10, also paper 78-1208 presented at the AIAA 11th Fluid and Plasma Dynamics Conference, Seattle, Wash., July 10-12, 1978.
- [8] M. Lesoinne, and C. Farhat, "Geometric Conservation Laws for Flow Problems with Moving Boundaries and Deformable Meshes and Their Impact on Aeroelastic Computations," *Computer Methods in Applied Mechanics and Engineering*, Vol. 134, pp. 71-90 (1996).
- [9] Rozhdestvenskii, and Yanenko, "Theory of Quasilinear Hyperbolic Partial Differential Equations," NAUKA, 1970.
- [10] R.W. MacCormack, and A.J.Paullay, "THE INFLUENCE OF THE COMPUTATIONAL MESH ON ACCURACY FOR INITIAL VALUE PROBLEMS WITH DISCONTINUOUS OR NONUNIQUE SOLUTIONS," *Computers and Fluids*, Vol. 2, pp. 339-361, Pergammon Press, 1974.
- [11] Klaus A. Hoffman. *Computational Fluid Dynamics for Engineers*. ISBN 0-9623731-4-1, LOC Card Number 89-80978, pp.171.
- [12] C. Hirsh. *NUMERICAL COMPUTATION OF INTERNAL AND EXTERNAL FLOWS*. Vol 2. John Wiley and Sons, ISBN 0 471 923516 (v.2), 1990.



- [13] P. L. Row, "A Survey of Upwind Differencing Techniques," in *Lecture Notes in Physics*, Vol. 323 (Springer-Verlag, New York/Berlin, 1989), p. 69.
- [14] Meng-Sing Liou, "A Sequel to AUSM: AUSM+," *Journal of Computational Physics*, **129**, 364-382 (1996), Article Number 0256.
- [15] S. Tatsumi, L. Martinelli, A. Jameson, "Design, Implementation, and Validation of Flux Limited Schemes for the Solution of the Navier-Stokes Equations," AIAA-94-0647.
- [16] Timothy J. Barth, "A 3-D Upwind Euler Solver for Unstructured Meshes," AIAA-91-1548-CP.
- [17] Steger, J.L., and Warming, R.F., "Flux vector splitting of the inviscid gas-dynamic equations with applications to finite difference methods," *Journal of Computational Physics*, **40**, 263-93.
- [18] Bram Van Leer, "Towards the Ultimate Conservative Difference Scheme. V. A Second-Order Sequel to Godunov's Method," *Journal of Computational Physics*, **32**, 101-136 (1979).
- [19] Guang-Shan Jiang and Chi-Wang Shu, "Efficient Implementation of Weighted ENO Schemes," *Journal of Computational Physics*, **126**, 202-228 (1996).
- [20] Tariq D. Aslam, "A Level Set Method for Tracking Discontinuities in Hyperbolic Conservation Laws I: Scalar Equations," UCLA CAM Report at <ftp://ftp.math.ucla.edu/pub/camreport/cam98-28.ps.gz>.
- [21] Rebecca M. Brannon, "Geometric Justification of Radial and Oblique Return Plasticity Algorithms," <http://me.umn.edu/rnbrann/RadialReturn.pdf>.
- [22] Timothy J. Barth and Dennis C. Jespersen, "The Design and Application of Upwind Schemes on Unstructured Meshes," AIAA-89-0366, 27<sup>th</sup> Aerospace and Sciences Meeting, Jan. 9-12, Reno, NV, 1989.

DISTRIBUTION LIST  
AFRL-MN-EG-TR-2001-7023

Defense Technical Information Center      1  
8725 John J. Kingman Road, Ste 0944  
Ft Belvoir, VA 22060-6218

Air University Library      1  
600 Chennault Circle  
Bldg 1405  
Maxwell AFB, AL 36112-6424

EGLIN AFB OFFICES:

AFRL/MN/CA-N      1  
AFRL/MNOC-1 (STINFO Office)      1  
AFRL/MNA      1  
AFRL/MNAC      1